Equilibria determination of elastic articulated duoskelion beams in 2D via a Riks-type algorithm

Emilio Barchiesi, Francesco Dell'Isola, Alberto M. Bersani, Emilio Turco

Equilibria determination of elastic articulated duoskelion beams in 2D via a Riks-type algorithm

Emilio Barchiesi [a], Francesco dell'Isola [a,b], Alberto M. Bersani [c], Emilio Turco [d,*]

[a] International Research Center on the Mathematics and Mechanics of Complex Systems (M&MOCS), University of L'Aquila, Italy
[b] Department of Civil, Construction-Architectural and Environmental Engineering (DICEAA), University of L'Aquila, Italy
[c] Dipartimento di Ingegneria Meccanica e Aerospaziale (DIMA), Sapienza University of Roma, Italy
[d] Department of Architecture, Design and Urban Planning (DADU), University of Sassari, Italy

A B S T R A C T

The overall behavior of an articulated beam structure constituted by elements arranged according to a specific chirality is studied. The structure as a whole, due to its slenderness and geometry, is called *duoskelion beam*. The name *duoskelion* is a neologism which is inspired by the Greek word δύοσκέλιον (two-legged). A discrete model for shearable beams, formulated recently, is exploited to investigate its mechanics. A purposely designed numerical scheme, adapting the Riks rationale, is used to calculate large displacement and deformation equilibria of duoskelion beams. Aimed at computing the current step correction, the Riks arc-length method is modified and made more efficient by applying a specific orthogonality condition, defined via the stiffness matrix, to an adapted extrapolation step. The robustness of the resulting scheme and its capability to follow equilibrium branches allows, in principle, for the exploration of the whole set of local energy minima in the introduced space of configurations, by using suitably modulated perturbative external loads. The developed numerical tool can be used to understand the mechanics of duoskelion beams. It is proved that there exists a stable principal equilibrium branch in which only compression is observed for any compression load. Additional stable equilibrium branches are found in compression such that the clamped–clamped compressed beam assumes a characteristic *S* shape which, upon reaching a critical load, is significantly amplified. A mechanically relevant stable equilibrium is also found in extension, being observed the *S*-shaped configuration experimentally found in Misra et al. (2020).

1. Introduction

Metamaterials theory [1,2] looks for microstructures synthesizing complex and exotic macroscopic behaviors [3,4]. A relevant exam ple of methodologies and results in metamaterials theory is given, as an instance, by so called pantographic metamaterials [5 7]: de sign and manufacturing [8 10], modeling [11 17] and experimental techniques [18,19] are all concurring to the conception of optimal engineering materials with specific target behaviors. Indeed, meta materials science is extremely interdisciplinary combining different fields in mechanics and data analysis like strain gradient [20,21] and generalized [22 24] continuum theories, digital image and volume correlation [25,26], innovative manufacturing processes, mathematical theories of elastic and dissipative media [27 30] and computational methods for elasticity and plasticity [31 34].

Aimed at finding a class of slender metamaterials [35,36] mi crostructures behaving chirally at macroscopic level [37], a specific articulated structure is introduced, which is constituted by a set of dis crete beam elements with graded extensional and bending stiffnesses. The microstructure is conceived in order to obtain chirality effects analogous to those already measured experimentally in [38], where the observation of an interesting and exotic stable equilibrium path is reported. Indeed, in extension tests performed by [38], a characteristic stable *S* shaped deformed equilibrium configuration is found when clamping clamping conditions are applied.

The conceived microstructure consists conceptually of two struc tural elements: rigid two legged bodies and purely extensible springs. These two kinds of elements are hinged together and interact through an elastic rotational spring opposing to their relative rotation (see Fig. 1). Because of its slenderness and cell geometry, the complex structure obtained by periodically repeating along the horizontal axis the duoskelion motif is referred to, as a whole, as *duoskelion beam*.

Aimed at fully investigating the mechanical behavior of duoskelion beams and at understanding its properties when regarded as a unique macroscopic non standard beam, a microscopic discrete model is intro duced. Such a model consists of a set of interconnected shearable, flex ible and extensible Timoshenko like elements. The employed discrete

* Corresponding author.
E-mail address: emilio.turco@uniss.it (E. Turco).

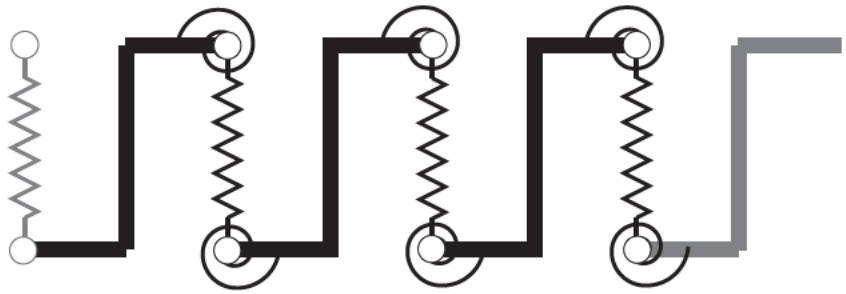

Fig. 1. Conceptual discrete duoskelion beam geometry and mechanics.

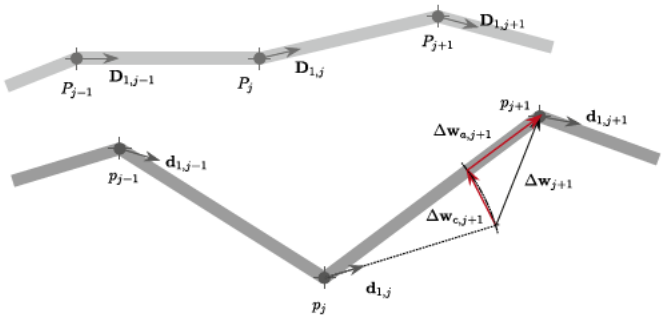

Fig. 2. Reference (light gray) and current (dark gray) configurations with related kinematic quantities. Geometrical meaning of stretch deformation $\Delta\mathbf{w}_{a,j+1}$ and shearing deformation $\Delta\mathbf{w}_{c,j+1}$ is given in red for the generic discrete Timoshenko-like element in plane considered in this work. (For interpretation of the references to color in this figure legend, the reader is referred to the web version of this article.)

formulation, which models the system with more (and more complex) elements than those in the conceptual description outlined above, considers suitable ratios between homologous, *e.g.* bending/bending, and non homologous, *e.g.* bending/shearing, stiffnesses to get such a conceptual description as a special case.

Such a formulation is computed by adapting the Riks rationale. More particularly, an orthogonality condition, defined via the stiffness matrix, is applied to an adapted extrapolation, giving a robust numer ical scheme which is naturally able to calculate, with no additional shrewdness, very stiff non linear problems with possibly multiple solu tions (being the applied displacements and/or forces the same) in the same equilibrium path. The intelligent use of modulated perturbative loads within this approach allows also for the computation of multiple solutions belonging to different equilibrium paths.

The plan of the work is the following one. In Section 2 the discrete Timoshenko like element is briefly introduced, as well as the geometry and discretization of the system and ratios between homologous and non homologous stiffnesses. In Section 3 the numerical scheme em ployed to solve the static equilibrium problem is described. Section 4 presents, discusses and interprets results of numerical tests in view of real world applications and continuum representation of duoskelion beams, also tracing connections with existing literature. Finally, in Section 5 conclusions are drawn and future outlooks of the work are given.

2. Mechanical model

A Timoshenko like beam in plane, see [39,40], is formulated dis cretely for arbitrarily large deformations as a finite set of connected straight links, see Fig. 2. Joints (equivalently, nodes) are numbered in such a way that adjacent joints are labeled with two consecutive natural numbers.

The current position of joint j is denoted with p_j and its reference position with P_j, being $j = 1, 2, \ldots, N_t$. Following the spirit of enriched continua, each joint is endowed with a unit vector, that for the generic joint j reads in the reference configuration as

$$\mathbf{D}_{1,j} = \frac{P_{j+1} - P_j}{\|P_{j+1} - P_j\|}\,. \tag{1}$$

Such a unit arrow is transformed in the current configuration into the unit arrow $\mathbf{d}_{1,j} = \mathbf{Q}_j\mathbf{D}_{1,j}$, being $\mathbf{Q}_j$ a proper orthogonal second rank rotation tensor. Therefore, reference and current configurations are determined, respectively, by the Lagrangian parameters $\{P_j, \mathbf{D}_{1,j}\}$ and $\{p_j, \mathbf{d}_{1,j}\}$.

Two strain measures, *i.e.* $\Delta\mathbf{w}_{j+1}$ and $\Delta\mathbf{Q}_{j+1}$, are defined for the generic index j according to Fig. 2. Particularly, the vector $\Delta\mathbf{w}_{j+1}$ is given by

$$\Delta\mathbf{w}_{j+1} = (p_{j+1} - p_j) - \|P_{j+1} - P_j\|\mathbf{Q}_j\mathbf{D}_{1,j}\,, \tag{2}$$

while the tensor $\Delta\mathbf{Q}_{j+1}$ is defined as

$$\Delta\mathbf{Q}_{j+1} = \mathbf{Q}_j^T\mathbf{Q}_{j+1} - \mathbf{I}\,, \tag{3}$$

with $\mathbf{I}$ being the identity second rank tensor. The strain vector $\Delta\mathbf{w}_{j+1}$ can be decomposed in two additive terms

$$\Delta\mathbf{w}_{a,j+1} = (p_{j+i} - p_j)\left(1 - \frac{\|P_{j+1} - P_j\|}{\|p_{j+1} - p_j\|}\right)\,, \tag{4}$$

$$\Delta\mathbf{w}_{c,j+1} = \Delta\mathbf{w}_{j+1} - \Delta\mathbf{w}_{a,j+1}\,. \tag{5}$$

Each quantity in Eqs. (4) and (5) is interpreted geometrically in Fig. 2. Indeed, it is easy to see that the norms of the strain measures in Eqs. (4) and (5) can be interpreted as measuring, respectively, the stretch (link's absolute change of length) and the shearing,[1] deformations of the link in between joints j and $j+1$. The quantity $\Delta\mathbf{Q}_j$ is a bending measure for the element formed by the two links joining, respectively, nodes $j+1/j$ and $j/j-1$. Indeed, for such an element bending is considered in the present discrete formulation as the relative rotation of $\mathbf{D}_{1,j-1}$ and $\mathbf{D}_{1,j}$, being the vectors $\mathbf{D}_{1,j-1}$ and $\mathbf{D}_{1,j}$ rotating into the vectors $\mathbf{d}_{1,j-1}$ and $\mathbf{d}_{1,j}$ in the current configuration, respectively. It is worth remarking that the quantity $\Delta\mathbf{Q}_j + \mathbf{I} = \mathbf{Q}_{j-1}^T\mathbf{Q}_j$ is a proper orthogonal tensor. If $\mathbf{Q}_{j-1} = \mathbf{Q}_j$ then $\Delta\mathbf{Q}_j$ is the null tensor.

Relationships between the independent Lagrangian parameters used to describe the motion, *i.e.* displacements and rotations of joints, and the chosen strain measures $\Delta\mathbf{w}_{a,j}$, $\Delta\mathbf{w}_{c,j}$ and $\Delta\mathbf{Q}_{j+1}$ have been given. The total deformation energy of the whole discrete Timoshenko like beam is given by the summation along the beam of the elementary contributions

$$E_{a,j} = \frac{k_a}{2}\|\Delta\mathbf{w}_{a,j+1}\|^2\,, \tag{6}$$

$$E_{b,j} = \frac{k_b}{2}\|\Delta\mathbf{Q}_{j+1}\|^2\,, \tag{7}$$

[1] Any measure of mismatch between link's and $\boldsymbol{D}_{1,j}$'s directions in the current configuration is considered to be a shearing deformation; remark that the shearing measure illustrated in Fig. 2 is a positive increasing function of the angle formed by these two directions only when such an angle ranges from 0° to 180° from 180° to 360°, etc.

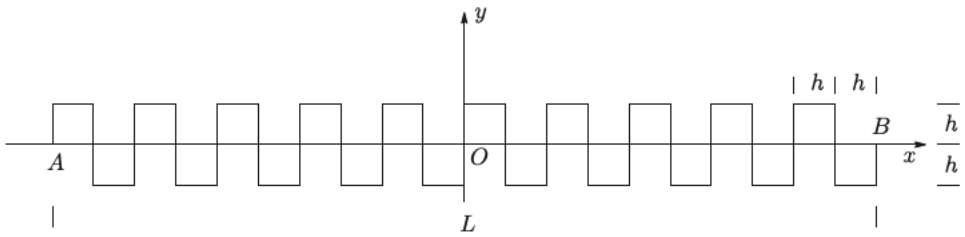

Fig. 3. Duoskelion beam geometry before discretization.

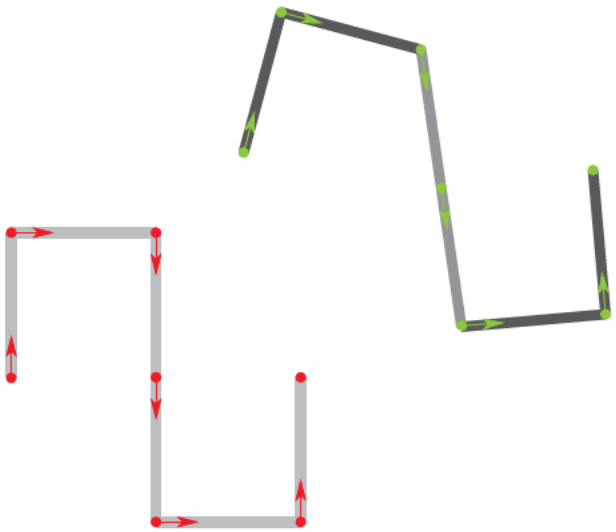

Fig. 4. Periodically repeated cell, *i.e.* duoskelion motif, in undeformed and deformed configurations as discretized by Timoshenko-like elements. Shearing stiffness is infinite throughout the whole beam. Links which are dark in the deformed configuration have infinite extensional stiffness. Elements formed by two adjacent links with same color in the deformed configuration have infinite bending stiffness. (For interpretation of the references to color in this figure legend, the reader is referred to the web version of this article.)

$$E_{c,j} = \frac{k_c}{2}\|\Delta \mathbf{w}_{c,j+1}\|^2, \tag{8}$$

where $\|\Delta \mathbf{w}_{a,j+1}\|$ and $\|\Delta \mathbf{w}_{c,j+1}\|$ are the Euclidean norms of the vectors $\Delta \mathbf{w}_{a,j+1}$ and $\Delta \mathbf{w}_{c,j+1}$, respectively, $\|\Delta \mathbf{Q}_{j+1}\|^2 = \mathrm{tr}(\Delta \mathbf{Q}_{j+1}^T \Delta \mathbf{Q}_{j+1})$, and k_a, k_b, and k_c are stiffness parameters[2] corresponding to stretch, bending and shearing deformations, respectively. Note that if E_a, E_b, and E_c are defined to be, respectively, the total extensional, bending, and shearing deformation energies, *i.e.* they are obtained by summing up, respectively, all elementary contributions in Eqs. (6), (7), and (8) along the beam, then the total deformation energy is given by $E_a + E_b + E_c$.

Remark also that, if $\mathbf{d}_{1,j}$ is required to be parallel to the link connecting nodes j and $j+1$ in the current configuration, then there is no shearing deformation and one retrieves a Hencky type discretization of the extensible Elastica which can be otherwise considered a generalization to finite deformations and extensible beams of Hencky's approximation of Euler Bernoulli beam model. Such a generalization is discussed, *e.g.*, in the work [41].

2.1. Geometry and ratios between stiffnesses

The duoskelion beam geometry shown in Fig. 3 is discretized by means of the Timoshenko like elements introduced above as shown in Fig. 4, *i.e.* one link for horizontal tracts and two links for vertical tracts, being the length of all links the same in the undeformed configuration. As mentioned in the Introduction, the microstructure which is going to be studied in this work consists actually in a special case, as it is meant to be made by rigid two legged bodies and purely extensible springs (see Fig. 1). Such a special case is not to be recovered by enforcing kinematic conditions, *i.e.* on strain measures and hence on kinematic quantities, but rather by letting for all links the shearing stiffness k_c tending to infinite.[3] Additionally, for selected links and elements, the extensional and bending stiffnesses, respectively, tend to infinite (see the deformed configuration in Fig. 4). Links which are dark in the deformed configuration have infinite extensional stiffness. Elements formed by two adjacent links with same color in the deformed configuration have infinite bending stiffness.

Clearly, all elements and links within the system must have, strictly speaking, finite stiffnesses. Indeed, those stiffnesses which should tend to infinite are considered to be much greater than those which should have a finite value. Numerical values for model parameters will be provided in the sequel.

3. Computation of the equilibrium path

Let the state (or, equivalently, the configuration) of the discrete system be uniquely determined by means of N_t Lagrangian parameters collected in $\boldsymbol{q}_t \in \mathbb{R}^{N_t}$, and let $\alpha \in \mathbb{R}$ be an external world interaction variable. Additionally, let the configuration $\boldsymbol{q}_t$ be split into two vectors, *i.e.* $\boldsymbol{q}_t = (\boldsymbol{q}, \boldsymbol{q}_{con})$, with $\boldsymbol{q} \in \mathbb{R}^N$ and $\boldsymbol{q}_{con} \in \mathbb{R}^{N_t - N}$ collecting, respectively, the free and constrained Lagrangian coordinates of the system. Assume that the constraints can be expressed in the form $\boldsymbol{q}_{con} = \boldsymbol{q}_{c0}$, with $\boldsymbol{q}_{c0}$ not depending on α. The considered discrete system is characterized by the total energy $E(\boldsymbol{q}, \alpha)$. There are many instances of $E(\boldsymbol{q}, \alpha)$ that could be analyzed. A few of them will now be recalled to familiarize the reader with the framework and prepare the field to the next section.

At first, one may assume $E(\boldsymbol{q}, \alpha)$ to be given by

$$E(\boldsymbol{q}, \alpha) = E^{\mathrm{def}}(\boldsymbol{q}, \boldsymbol{q}_{c0}) - \boldsymbol{Q}(\alpha) \cdot \boldsymbol{q}, \tag{9}$$

being E^{def} the deformation energy of the whole system, and $\boldsymbol{Q}(\alpha) \in \mathbb{R}^N$ the external dead load parametrized in terms of α. Remark that results of numerical simulations reported in the next section are obtained by considering the total energy in Eq. (9) and making, case by case, suitable choices for $\boldsymbol{q}_{c0}$ and $\boldsymbol{Q}(\alpha)$. A frequent choice for $\boldsymbol{Q}(\alpha)$ is $\boldsymbol{Q}(\alpha) = \alpha \widetilde{\boldsymbol{Q}}_1 + \widetilde{\boldsymbol{Q}}_2$, with the loading shape $\widetilde{\boldsymbol{Q}}_1 \in \mathbb{R}^N$ and the load $\widetilde{\boldsymbol{Q}}_2 \in \mathbb{R}^N$ not depending upon α. Indeed, in all numerical tests reported in this work, the dead load $\boldsymbol{Q}(\alpha)$ in Eq. (9) has been chosen to be as such.

A further instance of $E(\boldsymbol{q}, \alpha)$ can be provided by considering the vector of Lagrangian parameters $\boldsymbol{q}_t$ to be augmented as $(\boldsymbol{q}, \boldsymbol{q}_{con}, \boldsymbol{q}_e)$ by a subset of N_e constrained Lagrangian parameters collected in $\boldsymbol{q}_e \in \mathbb{R}^{N_e}$ that can be expressed as a given function $\boldsymbol{q}_e(\alpha)$ of α. A frequent choice for $\boldsymbol{q}_e(\alpha)$ is $\boldsymbol{q}_e(\alpha) = \alpha \boldsymbol{Q}_{1e} + \boldsymbol{Q}_{2e}$, with the configuration $\boldsymbol{Q}_{2e} \in \mathbb{R}^{N_e}$ and the constraint shape $\boldsymbol{Q}_e \in \mathbb{R}^{N_e}$ not depending upon α. Note that Lagrangian parameters collected in $\boldsymbol{q}_e$, that do not depend upon α, could be equivalently collected in $\boldsymbol{q}_c$ and vice versa.

[2] The dependence of stiffness parameters upon the index j has been omitted to lighten the notation.

[3] In this way, the unit arrow attached to each node will be co-axial to the adjacent right link.

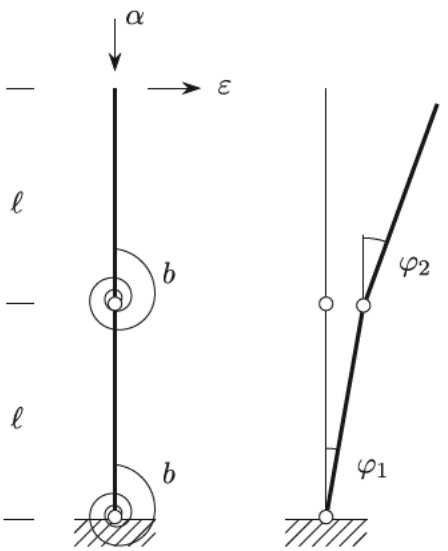

Fig. 5. Loading and kinematic conditions for the rigid-bar system considered to elucidate and exemplify the tangent stiffness-orthogonality constraint.

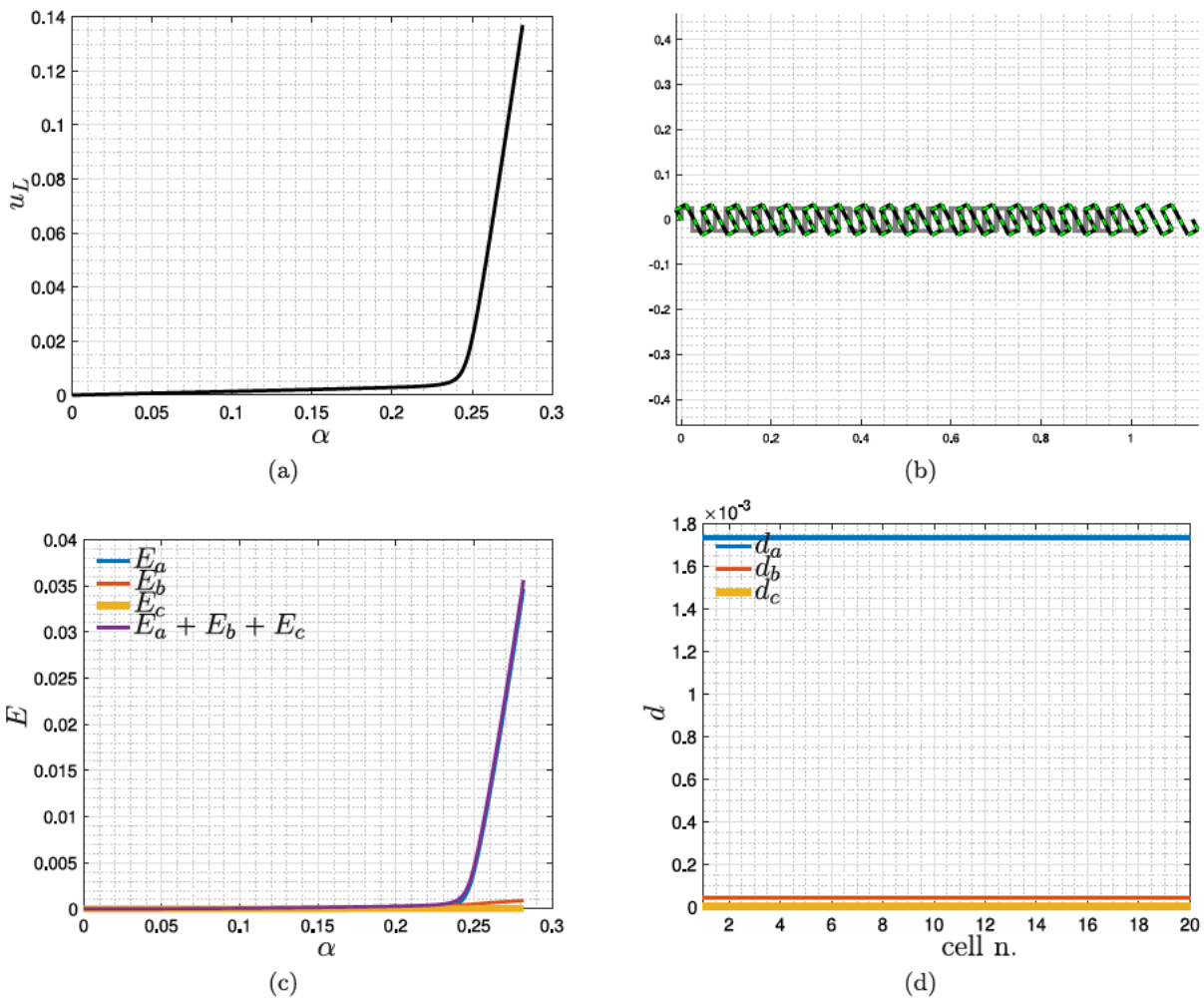

Fig. 6. Simply supported duoskelion beam formed by 20 cells subjected to traction force: equilibrium path (a), final deformation (b), energy evolution (c) and cell energy density (d). (For interpretation of the references to color in this figure legend, the reader is referred to the web version of this article.)

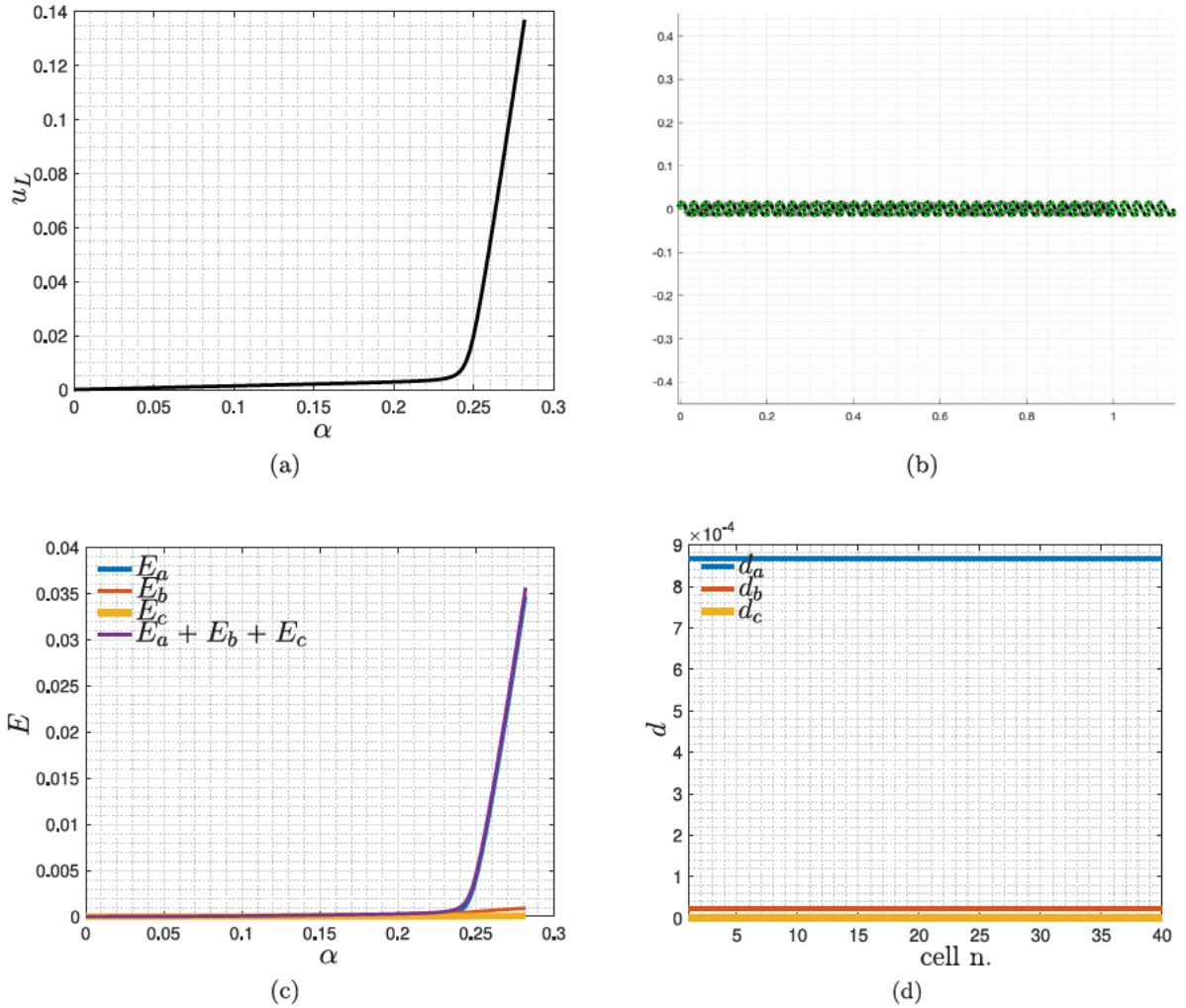

Fig. 7. Simply supported duoskelion beam formed by 40 cells subjected to traction force: equilibrium path (a), final deformation (b), energy evolution (c) and cell energy density (d). (For interpretation of the references to color in this figure legend, the reader is referred to the web version of this article.)

At this point, one may assume $E(\boldsymbol{q},\alpha)$ to be given by

$$E(\boldsymbol{q},\alpha) = E_e^{\text{def}}\left(\boldsymbol{q},\boldsymbol{q}_{c0},\boldsymbol{q}_e(\alpha)\right). \tag{10}$$

Obviously, one may consider a combination of the previous two examples and possibly add a further external world interaction term $\boldsymbol{q}\cdot\boldsymbol{Q}_2(\alpha)\boldsymbol{q}$ leading to

$$E(\boldsymbol{q},\alpha) = E_e^{\text{def}}(\boldsymbol{q},\boldsymbol{q}_{c0},\boldsymbol{q}_e(\alpha)) - \boldsymbol{Q}_1(\alpha)\cdot\boldsymbol{q} - \boldsymbol{q}\cdot\boldsymbol{Q}_2(\alpha)\boldsymbol{q}, \tag{11}$$

where the dead load $\boldsymbol{Q}_1$ has been complemented by a linear spring bed whose $N_e\times N_e$ matrix of stiffnesses $\boldsymbol{Q}_2$ is in general non diagonal and depending upon α.

For a given value of the parameter α, one seeks to find the (stable) equilibrium configurations, *i.e.* the stationary points of the total energy $E(\boldsymbol{q},\alpha)$ with respect to $\boldsymbol{q}$. Therefore, one looks for the solutions of the equilibrium equation

$$\boldsymbol{F}(\boldsymbol{q},\alpha) := \frac{\partial E}{\partial \boldsymbol{q}}(\boldsymbol{q},\alpha) = 0. \tag{12}$$

Henceforth, the symbol $\frac{\partial}{\partial \boldsymbol{x}}(\cdot)$ will denote the gradient of $(\cdot)$ with respect to the variables collected in the vector $\boldsymbol{x}$. Remark that also non minimum, *i.e.* non stable/marginally stable, stationary configurations for the total energy are solutions to Eq. (12), *i.e.* the *stiffness* matrix $\frac{\partial^2 E}{\partial \boldsymbol{q}\partial \boldsymbol{q}}$ is not necessarily positive definite. It is assumed that $\boldsymbol{F}(\boldsymbol{q}_0,\alpha_0) = 0$, *i.e.* that $(\boldsymbol{q}_0,\alpha_0)$ is an equilibrium configuration. The aim of the procedure, which is going to be described in the sequel, is to determine a whole curve Γ of equilibrium configurations in the space $(\boldsymbol{q},\alpha)$, *i.e.* an *equilibrium path*. Such a curve Γ is required to stem from $(\boldsymbol{q}_0,\alpha_0)$ and will be parametrized by a parameter σ that, generally speaking, cannot be expressed as a function of α. Indeed, the equilibrium curve Γ, which can be expressed as $(\boldsymbol{q}(\sigma),\alpha(\sigma))$, with $(\boldsymbol{q}(0),\alpha(0)) = (\boldsymbol{q}_0,\alpha_0)$, may include configurations with same α and different $\boldsymbol{q}$'s (and vice versa): being able of recovering this kind of equilibrium paths provides the motivation for not choosing α to parameterize the curve Γ.

Clearly, numerical algorithms only allow for the calculation of a finite number of approximate equilibrium configurations. Therefore, a sequence of steps $\left\{(\boldsymbol{q}_i,\alpha_i)\right\}_{i=0}^{N_{\max}}$ will be obtained at the end of the computation. In other words, the parameter σ, which is not generally speaking an arc length parameter in the sense of the Euclidean distance, is to be replaced with an index i denoting the number of steps done along the equilibrium curve Γ. For a fixed step i, an iteration procedure consisting of multiple sub steps will be needed, leading eventually to the estimation of point $i+1$ of the sequence $\left\{(\boldsymbol{q}_i,\alpha_i)\right\}_{i=0}^{N_{\max}}$ of equilibrium points. The index of this iteration procedure will be denoted by j in the sequel. In addition, the notation $(\cdot)|_{i,j}$ will denote the quantity $(\cdot)$ evaluated in $(\boldsymbol{q}_{i,j},\alpha_{i,j})$, where $(\boldsymbol{q}_{i,j},\alpha_{i,j})$ is the configu ration reached at sub step j of the iteration done passing from the last converged step $i-1$ to step i. The notation $(\cdot)|_i$ will denote the quantity $(\cdot)$ evaluated in $(\boldsymbol{q}_i,\alpha_i)$.

We shall now explain, given $(\boldsymbol{q}_i,\alpha_i)$, how one can pass from $(\boldsymbol{q}_{i+1,j},\alpha_{i+1,j})$ to $(\boldsymbol{q}_{i+1,j+1},\alpha_{i+1,j+1})$ and, eventually, to $(\boldsymbol{q}_{i+1},\alpha_{i+1})$ if a convergence criterion is fulfilled. Within the iterative procedure aimed

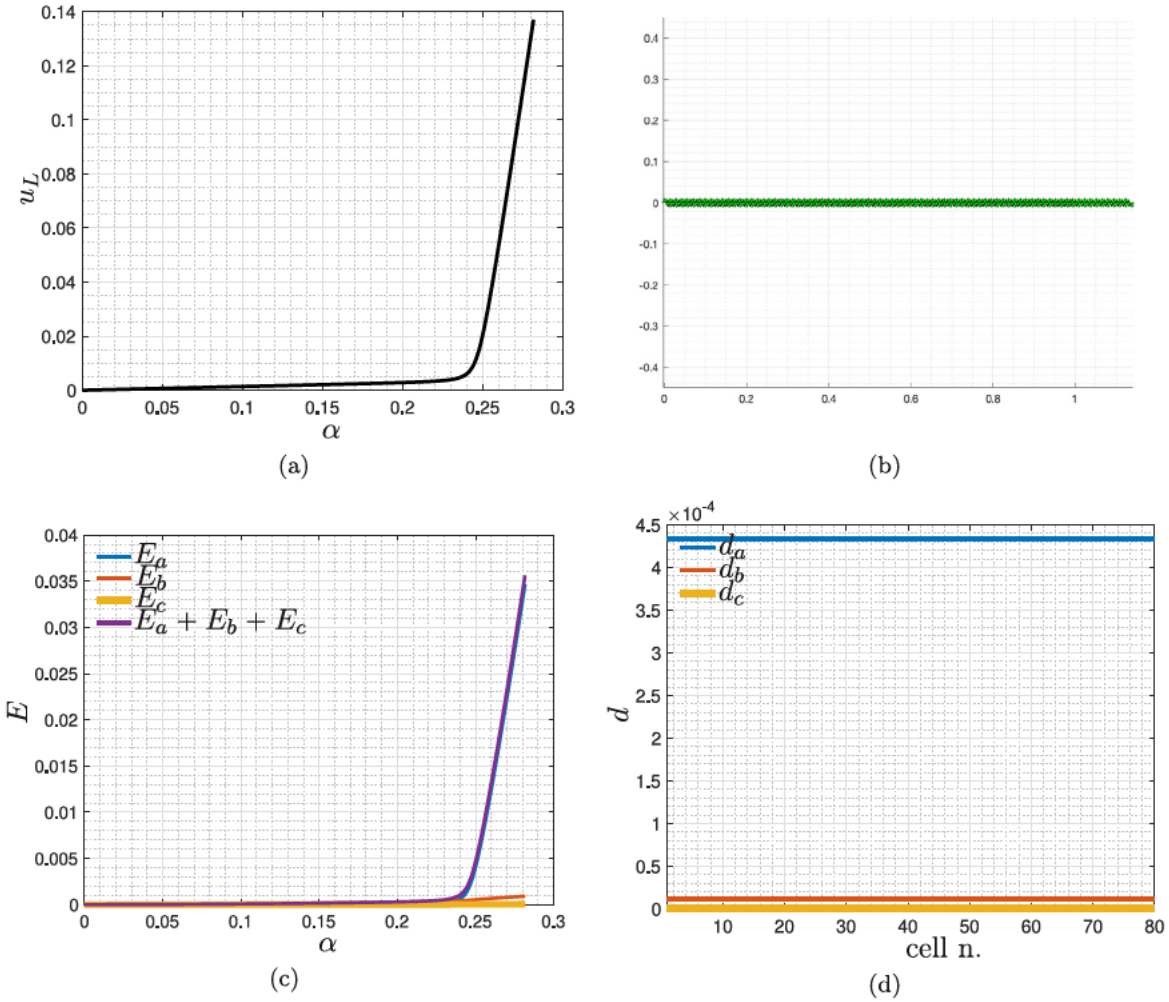

Fig. 8. Simply supported duoskelion beam formed by 80 cells subjected to traction force: equilibrium path (a), final deformation (b), energy evolution (c) and cell energy density (d). (For interpretation of the references to color in this figure legend, the reader is referred to the web version of this article.)

at passing from the last converged step i to step $i+1$, the index j ranges from zero to $r_{i+1}-1$, *i.e.*

$$\left(\boldsymbol{q}_{i+1,r_{i+1}}, \alpha_{i+1,r_{i+1}}\right) = \left(\boldsymbol{q}_{i+1}, \alpha_{i+1}\right),$$

this defining the quantity r_i. Preliminarily, the first order truncated Taylor expansion centered in $\left(\boldsymbol{q}_{i,j}, \alpha_{i,j}\right)$ of the quantity $\boldsymbol{F}$ evaluated in $\left(\boldsymbol{q}_{i+1,j+1}, \alpha_{i+1,j+1}\right)$ is provided

$$\boldsymbol{F}\left(\boldsymbol{q}_{i+1,j+1}, \alpha_{i+1,j+1}\right) \approx \boldsymbol{F}\left(\boldsymbol{q}_{i+1,j}, \alpha_{i+1,j}\right) + \left.\frac{\partial \boldsymbol{F}}{\partial \boldsymbol{q}}\right|_{i+1,j} \boldsymbol{q}^c_{i+1,j+1} + \left.\frac{\partial \boldsymbol{F}}{\partial \alpha}\right|_{i+1,j} \alpha^c_{i+1,j+1}, \tag{13}$$

where the configuration $\left(\boldsymbol{q}_{i+1,j+1}, \alpha_{i+1,j+1}\right)$ has been additively decomposed as the summation between the non equilibrium configuration $\left(\boldsymbol{q}_{i+1,j}, \alpha_{i+1,j}\right)$ and a correction $\left(\boldsymbol{q}^c_{i+1,j+1}, \alpha^c_{i+1,j+1}\right)$, *i.e.* the sub step correction is defined to be such that

$$\boldsymbol{q}_{i+1,j+1} = \boldsymbol{q}_{i+1,j} + \boldsymbol{q}^c_{i+1,j+1}, \tag{14}$$

$$\alpha_{i+1,j+1} = \alpha_{i+1,j} + \alpha^c_{i+1,j+1}. \tag{15}$$

The non equilibrium configuration $\left(\boldsymbol{q}_{i+1,j}, \alpha_{i+1,j}\right)$ reached at sub step j is further additively decomposed as

$$\boldsymbol{q}_{i+1,j} = \boldsymbol{q}_i + \Delta \boldsymbol{q}_{i+1,j}, \tag{16}$$

$$\alpha_{i+1,j} = \alpha_i + \Delta \alpha_{i+1,j}. \tag{17}$$

This latter decomposition is indeed a definition for $\Delta \boldsymbol{q}_{i+1,j}$. Such a quantity has been introduced as it plays a relevant role in the numerical algorithm. Owing to Eqs. (14),(15) and Eqs. (16), (17), the quantities $\boldsymbol{q}_{i+1,j+1}$ and $\alpha_{i+1,j+1}$ can be re written in incremental form as

$$\boldsymbol{q}_{i+1,j+1} = \boldsymbol{q}_i + \Delta \boldsymbol{q}_{i+1,j} + \boldsymbol{q}^c_{i+1,j+1}, \tag{18}$$

$$\alpha_{i+1,j+1} = \alpha_i + \Delta \alpha_{i+1,j} + \alpha^c_{i+1,j+1}, \tag{19}$$

or, equivalently, as

$$\boldsymbol{q}_{i+1,j+1} = \boldsymbol{q}_i + \Delta \boldsymbol{q}_{i+1,0} + \sum_{h=1}^{j+1} \boldsymbol{q}^c_{i+1,h}, \tag{20}$$

$$\alpha_{i+1,j+1} = \alpha_i + \Delta \alpha_{i+1,0} + \sum_{h=1}^{j+1} \alpha^c_{i+1,h}. \tag{21}$$

Enforcing $\left(\boldsymbol{q}_{i,j+1}, \alpha_{i,j+1}\right)$ to be an equilibrium point, *i.e.* $\boldsymbol{F}(\boldsymbol{q}_{i,j+1}, \alpha_{i,j+1}) = 0$, Eq. (13) gives

$$0 \approx \boldsymbol{F}\left(\boldsymbol{q}_{i+1,j}, \alpha_{i+1,j}\right) + \left.\frac{\partial \boldsymbol{F}}{\partial \boldsymbol{q}}\right|_{i+1,j} \boldsymbol{q}^c_{i+1,j+1} + \left.\frac{\partial \boldsymbol{F}}{\partial \alpha}\right|_{i+1,j} \alpha^c_{i+1,j+1}. \tag{22}$$

As mentioned earlier, the variable α is not used to parameterize the equilibrium curve Γ, *i.e.* $\alpha^c_{i+1,j+1}$ is not chosen arbitrarily in Eq. (22). Therefore, the condition (22) alone is not sufficient to allow for the computation of the corrections $\boldsymbol{q}^c_{i+1,j+1}$ and $\alpha^c_{i+1,j+1}$. It is for this very reason that an additional condition is introduced, which is called the

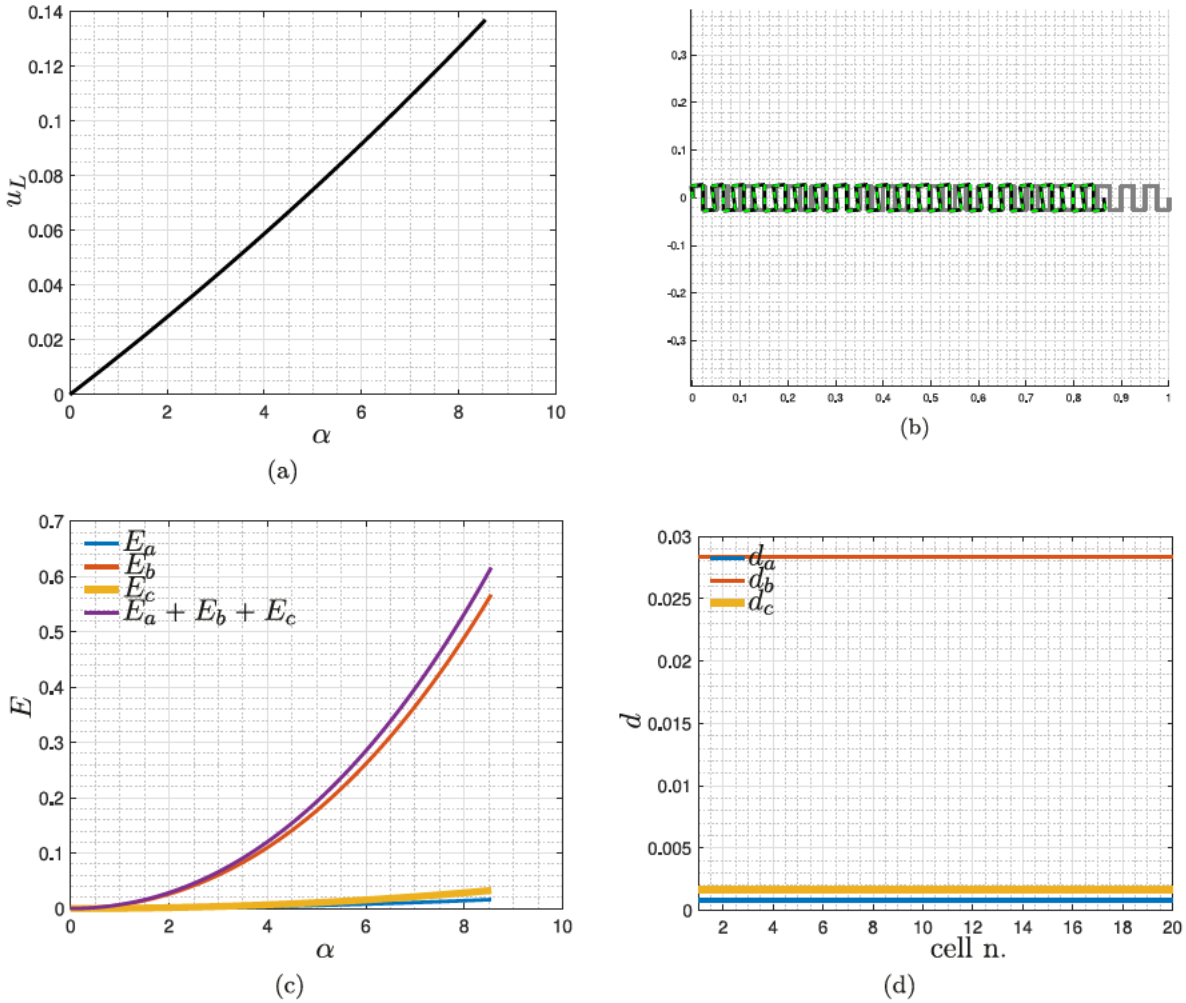

Fig. 9. Simply supported duoskelion beam formed by 20 cells subjected to compression force: equilibrium path (a), final deformation (b), energy evolution (c) and cell energy density (d).

tangent stiffness orthogonality condition

$$\Delta \boldsymbol{q}_{i+1,j} \cdot \left.\frac{\partial \boldsymbol{F}}{\partial \boldsymbol{q}}\right|_{i+1,j} \boldsymbol{q}^c_{i+1,j+1} = 0\,. \tag{23}$$

Before making use of such a condition it is noted that multiplying both sides of Eq. (22) by $\Delta \boldsymbol{q}_{i+1,j}$ allows to obtain the following equation

$$0 \approx \Delta \boldsymbol{q}_{i+1,j} \cdot \boldsymbol{F}\left(\boldsymbol{q}_{i+1,j}, \alpha_{i+1,j}\right) + \Delta \boldsymbol{q}_{i+1,j} \cdot \left.\frac{\partial \boldsymbol{F}}{\partial \boldsymbol{q}}\right|_{i+1,j} \boldsymbol{q}^c_{i+1,j+1} + \Delta \boldsymbol{q}_{i+1,j} \cdot \left.\frac{\partial \boldsymbol{F}}{\partial \alpha}\right|_{i+1,j} \alpha^c_{i+1,j+1}\,, \tag{24}$$

which, taking into account the orthogonality condition in Eq. (23), leads to a formula for $\alpha^c_{i+1,j+1}$ in terms of known quantities only

$$\alpha^c_{i+1,j+1} = -\frac{\Delta \boldsymbol{q}_{i+1,j} \cdot \boldsymbol{F}(\boldsymbol{q}_{i+1,j}, \alpha_{i+1,j})}{\Delta \boldsymbol{q}_{i+1,j} \cdot \left.\frac{\partial \boldsymbol{F}}{\partial \alpha}\right|_{i+1,j}}\,. \tag{25}$$

Substituting the value of $\alpha^c_{i+1,j+1}$ given by Eq. (25) into Eq. (22) gives

$$0 \approx \boldsymbol{F}\left(\boldsymbol{q}_{i+1,j}, \alpha_{i+1,j}\right) + \left.\frac{\partial \boldsymbol{F}}{\partial \boldsymbol{q}}\right|_{i+1,j} \boldsymbol{q}^c_{i+1,j+1} - \left.\frac{\partial \boldsymbol{F}}{\partial \alpha}\right|_{i+1,j} \frac{\Delta \boldsymbol{q}_{i+1,j} \cdot \boldsymbol{F}(\boldsymbol{q}_{i+1,j}, \alpha_{i+1,j})}{\Delta \boldsymbol{q}_{i+1,j} \cdot \left.\frac{\partial \boldsymbol{F}}{\partial \alpha}\right|_{i+1,j}}\,, \tag{26}$$

and, therefore, by simple algebraic manipulations, the sought correction $\boldsymbol{q}^c_{i+1,j+1}$ can be computed in terms of known quantities only as

$$\boldsymbol{q}^c_{i+1,j+1} \approx \left(\left.\frac{\partial \boldsymbol{F}}{\partial \boldsymbol{q}}\right|_{i+1,j}\right)^{-1} \left[\left.\frac{\partial \boldsymbol{F}}{\partial \alpha}\right|_{i+1,j} \frac{\Delta \boldsymbol{q}_{i+1,j} \cdot \boldsymbol{F}(\boldsymbol{q}_{i+1,j}, \alpha_{i+1,j})}{\Delta \boldsymbol{q}_{i+1,j} \cdot \left.\frac{\partial \boldsymbol{F}}{\partial \alpha}\right|_{i+1,j}} - \boldsymbol{F}\left(\boldsymbol{q}_{i+1,j}, \alpha_{i+1,j}\right)\right], \tag{27}$$

under the assumption that the matrix $\left.\frac{\partial \boldsymbol{F}}{\partial \boldsymbol{q}}\right|_{i+1,j}$ has non zero determinant.

According to Eqs. (20) and (21), it is needed to specify the quantities $\Delta \boldsymbol{q}_{i+1,0}$ and $\Delta \alpha_{i,0}$, which control the sub step 0 of the iterative procedure aimed at passing from the last converged step i to step $i+1$. Such quantities are chosen as follows

$$\Delta \boldsymbol{q}_{i+1,0} = \delta_{i+1}(\boldsymbol{q}_i - \boldsymbol{q}_{i-1})\,, \tag{28}$$

$$\Delta \alpha_{i+1,0} = \delta_{i+1}(\alpha_i - \alpha_{i-1})\,, \tag{29}$$

where the factor δ_{i+1} is given by

$$\delta_{i+1} = 1 - \frac{r_i - e}{r_i + e}\,, \tag{30}$$

being the parameter e the value expected, on average, for r_i's. The parameter e is chosen at the beginning of the algorithm and kept fixed throughout the whole computation. Remark that δ_{i+1} is an amplification/contraction factor which adapts the length of the initial sub step (*i.e.* sub step 0), which consists thus in a scaled extrapolation. Indeed, being r_i and e positive, according to Eq. (30) the quantity δ_{i+1} is always greater than zero and, in particular, it is (a) greater than one when r_i is less than e, (b) equal to one when r_i equals e, and (less than one when r_i is greater than e. Clearly, when $i = 0$, Eqs. (28), (29), and (30) do not apply. Indeed, it is assumed that only one equilibrium point, *i.e.* (q_0, α_0), is known at the beginning of the algorithm and r_0 is not defined as well.

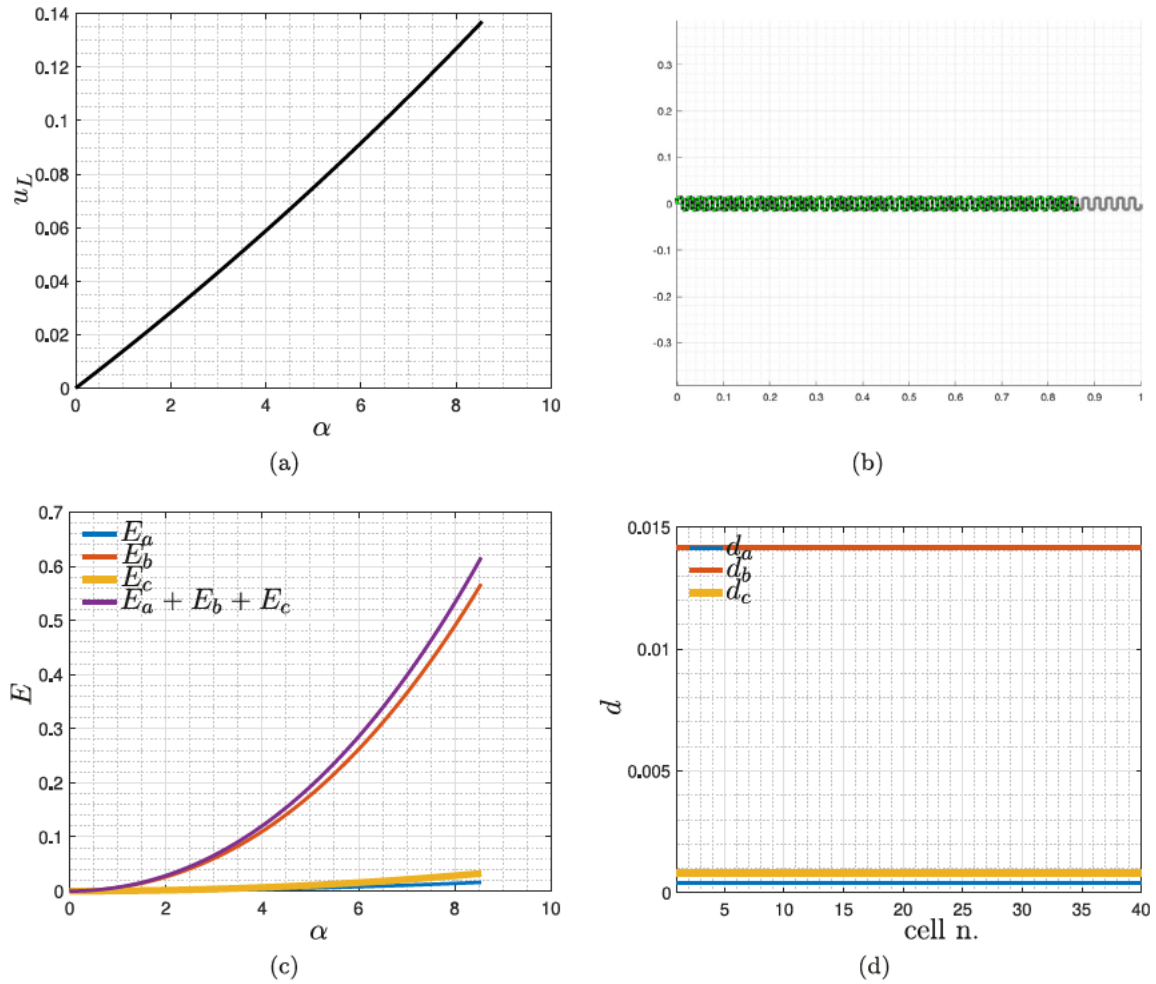

Fig. 10. Simply supported duoskelion beam formed by 40 cells subjected to compression force: equilibrium path (a), final deformation (b), energy evolution (c) and cell energy density (d).

The quantities $\Delta \boldsymbol{q}_{1,0}$ and $\Delta \alpha_{1,0}$ are then found as follows. The quantity $\Delta \alpha_{1,0}$ is chosen at the beginning of the algorithm, while the quantity $\Delta \boldsymbol{q}_{1,0}$ is found by applying Newton's method. The following truncated first order Taylor expansion is considered

$$\boldsymbol{F}(\boldsymbol{q}_{1,0}, \alpha_{1,0}) \approx \boldsymbol{F}(\boldsymbol{q}_0, \alpha_0) + \left.\frac{\partial \boldsymbol{F}}{\partial \boldsymbol{q}}\right|_0 \Delta \boldsymbol{q}_{1,0} + \left.\frac{\partial \boldsymbol{F}}{\partial \alpha}\right|_0 \Delta \alpha_{1,0} \,. \tag{31}$$

Reminding that $\boldsymbol{F}(\boldsymbol{q}_0, \alpha_0) = 0$, and enforcing $(\boldsymbol{q}_{1,0}, \alpha_{1,0})$ to be an equilibrium point, *i.e.* $\boldsymbol{F}(\boldsymbol{q}_{1,0}, \alpha_{1,0}) = 0$, the formula

$$\Delta \boldsymbol{q}_{1,0} = -\left(\left.\frac{\partial \boldsymbol{F}}{\partial \boldsymbol{q}}\right|_0\right)^{-1} \left.\frac{\partial \boldsymbol{F}}{\partial \alpha}\right|_0 \Delta \alpha_{1,0} \,, \tag{32}$$

is obtained for $\Delta \boldsymbol{q}_{1,0}$ under the assumption that the matrix $\left.\frac{\partial \boldsymbol{F}}{\partial \boldsymbol{q}}\right|_0$ has non zero determinant.

At this point, the convergence criterion which allows to establish whether the configuration $(\boldsymbol{q}_{i+1,j+1}, \alpha_{i+1,j+1})$ is a converged, *i.e.* equilibrium, one is to be presented. Clearly, there are many possible criteria, the most trivial ones being based on (modified) Euclidean norms of the (relative, for two consecutive sub steps) residual equilibrium vector $\boldsymbol{F}(\boldsymbol{q}_{i+1,j}, \alpha_{i+1,j})$ or on (modified) Euclidean norms of the relative solution for two consecutive sub steps. The criterion employed herein follows the spirit of the energy norm criterion mentioned in [42, pag. 31, Eq. 47].

Let the quantity $W_{i+1,j+1}$ be defined as the absolute value of the work done by the residual $\boldsymbol{F}(\boldsymbol{q}_{i+1,j}, \alpha_{i+1,j})$ on the correction $\boldsymbol{q}^c_{i+1,j+1}$, *i.e.*

$$W_{i+1,j+1} = \left|\boldsymbol{F}(\boldsymbol{q}_{i+1,j}, \alpha_{i+1,j}) \cdot \boldsymbol{q}^c_{i+1,j+1}\right| .$$

The configuration $(\boldsymbol{q}_{i+1,j}, \alpha_{i+1,j})$ is considered as converged if the condition

$$W_{i+1,j+1} < \eta \left|\boldsymbol{F}(\boldsymbol{q}_i, \alpha_i) \cdot \Delta \boldsymbol{q}_{i+1,0}\right| ,$$

is met, with $\eta \in (0, 1]$ a quantity chosen at the beginning of the algorithm. It is now possible to write the pseudo code of the algorithm depicted above.

(a) **define** $\Delta \alpha_{1,0}$, e, η and $N_{\max}$
(b) **input** $\boldsymbol{q}_0$ and α_0
(c) $\Delta \boldsymbol{q}_{1,0} = -\left(\left.\frac{\partial \boldsymbol{F}}{\partial \boldsymbol{q}}\right|_0\right)^{-1} \left.\frac{\partial \boldsymbol{F}}{\partial \alpha}\right|_0 \Delta \alpha_{0,0}$
(d) **for** $i = 0$ to $i = N_{\max} - 1$
  (a) **if** $i > 0$
    i. $\delta_{i+1} = 1 - \frac{j-e}{j+e}$
    ii. $\Delta \boldsymbol{q}_{i+1,0} = \delta_{i+1}(\boldsymbol{q}_i - \boldsymbol{q}_{i-1})$
    iii. $\Delta \alpha_{i+1,0} = \delta_{i+1}(\alpha_i - \alpha_{i-1})$
  (b) **else**
  (c) **end**
  (d) $j = 0$
  (e) **do**

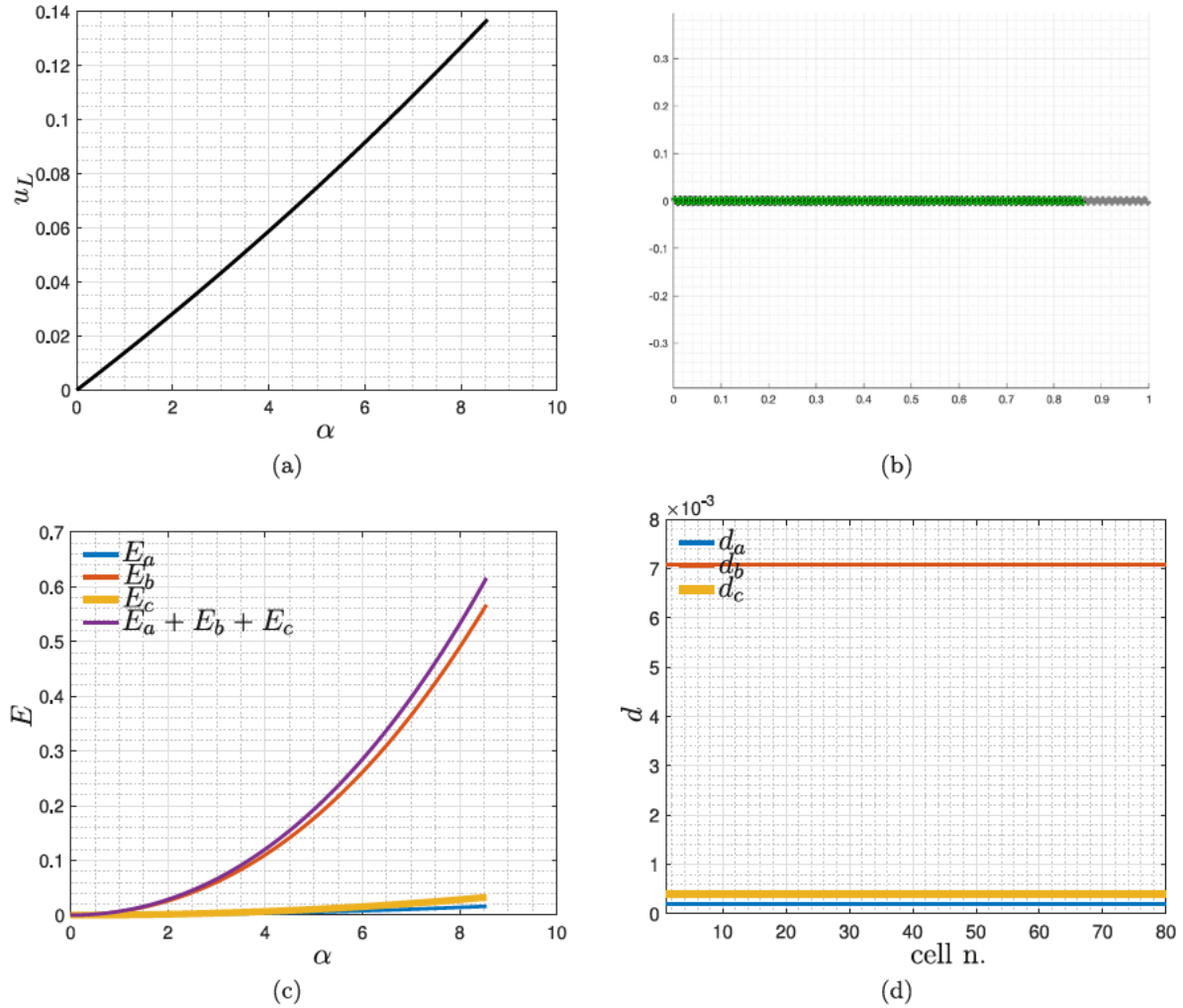

Fig. 11. Simply supported duoskelion beam formed by 80 cells subjected to compression force: equilibrium path (a), final deformation (b), energy evolution (c) and cell energy density (d).

i. $$\boldsymbol{q}^c_{i+1,j+1} = \left(\left.\frac{\partial \boldsymbol{F}}{\partial \boldsymbol{q}}\right|_{i+1,j}\right)^{-1} \times \left[\left.\frac{\partial \boldsymbol{F}}{\partial \alpha}\right|_{i+1,j} \frac{\Delta \boldsymbol{q}_{i+1,j} \cdot \boldsymbol{F}(\boldsymbol{q}_{i+1,j}, \alpha_{i+1,j})}{\Delta \boldsymbol{q}_{i+1,j} \cdot \left.\frac{\partial \boldsymbol{F}}{\partial \alpha}\right|_{i+1,j}} - \boldsymbol{F}\left(\boldsymbol{q}_{i+1,j}, \alpha_{i+1,j}\right)\right]$$

ii. $$\alpha^c_{i+1,j+1} = -\frac{\Delta \boldsymbol{q}_{i+1,j} \cdot \boldsymbol{F}(\boldsymbol{q}_{i+1,j}, \alpha_{i+1,j})}{\Delta \boldsymbol{q}_{i+1,j} \cdot \left.\frac{\partial \boldsymbol{F}}{\partial \alpha}\right|_{i+1,j}}$$

iii. $\boldsymbol{q}_{i+1,j+1} = \boldsymbol{q}_{i+1,j} + \boldsymbol{q}^c_{i+1,j+1}$

iv. $\alpha_{i+1,j+1} = \alpha_{i+1,j} + \alpha^c_{i+1,j+1}$

v. $j = j + 1$

(f) **while** $W_{i+1,j} \geq \eta \left|\boldsymbol{F}\left(\boldsymbol{q}_i, \alpha_i\right) \cdot \Delta \boldsymbol{q}_{i+1,0}\right|$

(g) $\boldsymbol{q}_{i+1} = \boldsymbol{q}_{i+1,j}$

(h) $\alpha_{i+1} = \alpha_{i+1,j}$

(e) **end**

The algorithm exposed in the foregoing is a generalization of many scientific contributions following the seminal idea reported in Riks' initial work, see [43]. Among the several papers published successively, the following ones are suggested to the interested readers: [44] for a geometric interpretation of the arc length method, [45] for the use of an adaptive arc length step, and Wriggers' book [46] where a comparison with different numerical strategies is also reported. Finally, in the work [26] Riks' basic idea is extended to the case when some constrained kinematical descriptors (displacements) can be expressed in terms of the parameter α as discussed above.

3.1. A note on the tangent stiffness orthogonality condition

In this subsection, the condition in Eq. (23) is to be elaborated. Note that the tangent stiffness orthogonality condition used above is only a possible choice that one might do to balance equations and unknowns when the equilibrium path is not parametrized over the external world interaction variable; indeed, Riks' original choice was a geometrical, *i.e.* based on the standard Euclidean inner product, orthogonality condition between the extrapolation $\Delta \boldsymbol{q}_{i+1,j}$ and the correction $\boldsymbol{q}^c_{i+1,j+1}$. In the Authors' opinion, the main advantage of the tangent stiffness orthogonality condition over other possible choices is that it leads to a very simple formula for $\alpha^c_{i+1,j+1}$ which involves only the ratio between inner products of known vectors, thus avoiding to solve a system of equations, *i.e.* to invert a matrix.

Some simple manipulations suggest an evocative mechanical interpretation of the tangent stiffness orthogonality condition. Indeed, such a condition, owing to the symmetry of the stiffness matrix $\frac{\partial \boldsymbol{F}}{\partial \boldsymbol{q}}$, can be re written as

$$\boldsymbol{q}^c_{i+1,j+1} \cdot \left.\frac{\partial \boldsymbol{F}}{\partial \boldsymbol{q}}\right|_{i+1,j} \Delta \boldsymbol{q}_{i+1,j} = 0\,. \tag{33}$$

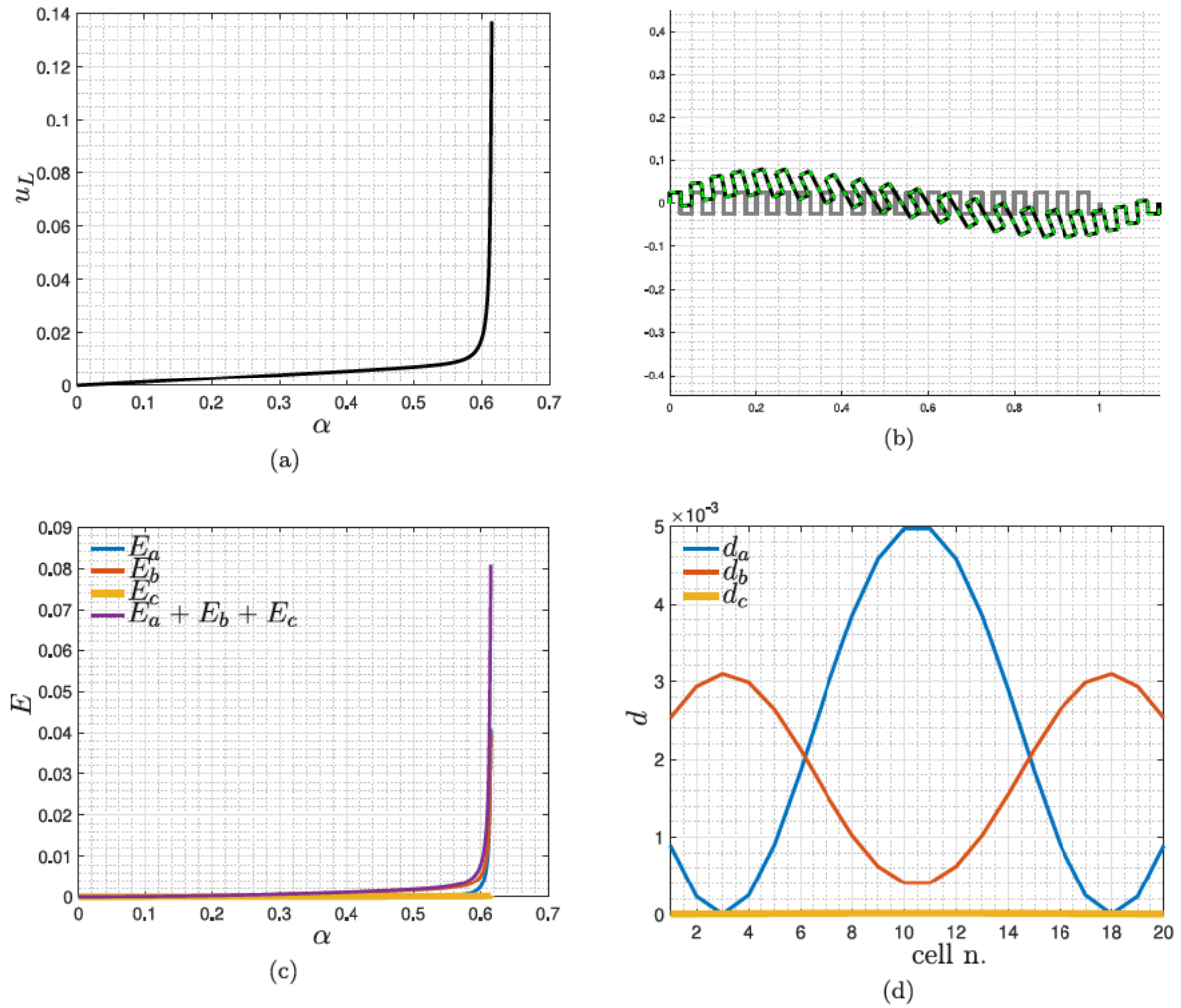

Fig. 12. Duoskelion beam formed by 20 cells subjected to clamp-sliding support kinematic conditions and traction force: equilibrium path (a), final deformation (b), energy evolution (c) and cell energy density (d).

Assume that the total energy $E(\boldsymbol{q},\alpha)$ of the system can be written as in Eq. (9), *i.e.* constraints on (a subset of) Lagrangian parameters are not parametrized on α and, therefore, $E(\boldsymbol{q},\alpha) = E^{\text{def}}(\boldsymbol{q},\boldsymbol{q}_{c0}) - \boldsymbol{Q}(\alpha)\cdot\boldsymbol{q}$. The quantity $\boldsymbol{S}(\boldsymbol{q})$, called *structural reaction*, is defined as $\boldsymbol{S}(\boldsymbol{q}) = \dfrac{\partial E^{\text{def}}}{\partial \boldsymbol{q}}$. Therefore, by using a Taylor expansion with respect to $\Delta\boldsymbol{q}_{i+1,j}$ truncated at first order and centered in $\boldsymbol{q}_{i+1,j}$, it is possible to write the term $\left.\dfrac{\partial \boldsymbol{F}}{\partial \boldsymbol{q}}\right|_{i+1,j}\Delta\boldsymbol{q}_{i+1,j}$ in Eq. (33) as $\boldsymbol{S}(\boldsymbol{q}_{i+1,j}) - \boldsymbol{S}(\boldsymbol{q}_i)$, and hence the tangent stiffness orthogonality condition can be rewritten, up to $o(\Delta\boldsymbol{q}_{i+1,j})$, as

$$\boldsymbol{q}^c_{i+1,j+1}\cdot\left(\boldsymbol{S}(\boldsymbol{q}_{i+1,j}) - \boldsymbol{S}(\boldsymbol{q}_i)\right) = 0\,, \tag{34}$$

or, equivalently, since $(\boldsymbol{q}_i,\alpha_i)$ is an equilibrium point, *i.e.* $\boldsymbol{S}(\boldsymbol{q}_i) = \boldsymbol{Q}(\alpha_i)$, it can be re written as

$$\boldsymbol{q}^c_{i+1,j+1}\cdot\left(\boldsymbol{S}(\boldsymbol{q}_{i+1,j}) - \boldsymbol{Q}(\alpha_i)\right) = 0\,. \tag{35}$$

Therefore, the correction $\boldsymbol{q}^c_{i+1,j+1}$ is chosen as to fulfill the Euclidean orthogonality condition with respect to $\left(\boldsymbol{S}(\boldsymbol{q}_{i+1,j}) - \boldsymbol{Q}(\alpha_i)\right)$, *i.e.* the cor rection $\boldsymbol{q}^c_{i+1,j+1}$ is such that the unbalanced force $\left(\boldsymbol{S}(\boldsymbol{q}_{i+1,j}) - \boldsymbol{Q}(\alpha_i)\right)$ does zero work on it.

A simple example consisting in a system with two degrees of free dom is now to be presented to clarify and give an insight into the remarks above. The rigid bar system in Fig. 5 is considered. Loading and kinematic conditions in Fig. 5 can be regarded as a coarse approx imation of an axially loaded Elastica column with a transverse load imperfection aimed at reproducing a small, yet non zero, eccentricity of the compression load. Indeed, two initially aligned rigid straight links are connected with elastic hinges having stiffness b. The loading conditions consists of a compression force α and a tip transversal force ε representing a load imperfection.

The free, *i.e.* not constrained, Lagrangian parameters for this system are considered to be the angles φ_1 and φ_2, *i.e.* $\boldsymbol{q} = (\varphi_1,\varphi_2)$, see Fig. 5. To describe completely the kinematics of the system, an additional (constrained) variable must be considered like, *e.g.*, the displacement of the bottom node, which is constrained to be vanishing. In other words, the angles φ_1 and φ_2 provide the configuration of the system up to a rigid translation. The energy of the system is defined as

$$\begin{aligned} E(\boldsymbol{q},\alpha) = {} & \frac{1}{2}b\varphi_1^2 + \frac{1}{2}b(\varphi_2-\varphi_1)^2 + \\ & - \alpha\ell\left((1-\cos\varphi_1) + (1-\cos\varphi_2)\right) - \varepsilon\ell(\sin\varphi_1 + \sin\varphi_2)\,. \end{aligned} \tag{36}$$

The total energy completely characterizes the system and all needed quantities can be derived starting from it. Remark that, the total deformation energy of the system does not depend on the quantity α, *i.e.* there are no constraints parametrized over the external world interaction variable. Note that the dead load $\boldsymbol{Q}(\alpha)$ can be expressed in the form $\alpha\widetilde{\boldsymbol{Q}}_1 + \widetilde{\boldsymbol{Q}}_2$, where the quantities $\widetilde{\boldsymbol{Q}}_1$ and $\widetilde{\boldsymbol{Q}}_2$ are given by

$$\widetilde{\boldsymbol{Q}}_1 = \ell\begin{bmatrix}\sin\varphi_1\\ \sin\varphi_2\end{bmatrix}, \qquad \widetilde{\boldsymbol{Q}}_2 = \varepsilon\ell\begin{bmatrix}\cos\varphi_1\\ \cos\varphi_2\end{bmatrix}. \tag{37}$$

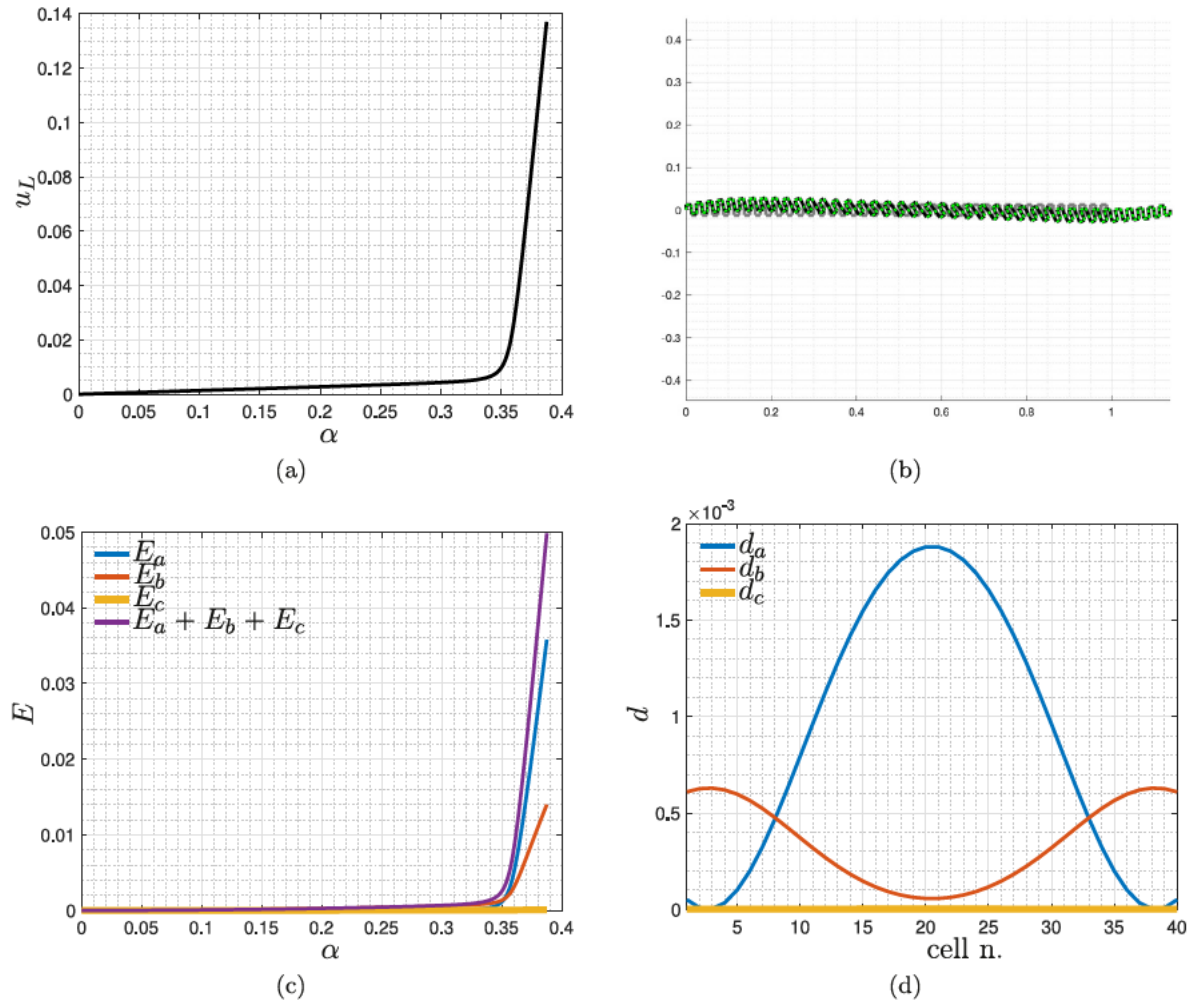

Fig. 13. Duoskelion beam formed by 40 cells subjected to clamp-sliding support kinematic conditions and traction force: equilibrium path (a), final deformation (b), energy evolution (c) and cell energy density (d).

Omitting indices i, $i+1$, j and $j+1$ for the variables φ_1 and φ_2 aimed at lightening the notation,[4] the structural reaction $\boldsymbol{S}(\boldsymbol{q}_{i+1,j})$ is given by

$$\boldsymbol{S}(\boldsymbol{q}_{i+1,j}) = b \begin{bmatrix} 2(\varphi_1 + \Delta\varphi_1) - (\varphi_2 + \Delta\varphi_2) \\ \varphi_2 + \Delta\varphi_2 - (\varphi_1 + \Delta\varphi_1) \end{bmatrix}, \tag{38}$$

and is obviously independent of α. Hence, Eq. (33) for this case reads as

$$\begin{bmatrix} \varphi_1^c \\ \varphi_2^c \end{bmatrix} \cdot \left(b \begin{bmatrix} 2(\varphi_1 + \Delta\varphi_1) - (\varphi_2 + \Delta\varphi_2) \\ \varphi_2 + \Delta\varphi_2 - (\varphi_1 + \Delta\varphi_1) \end{bmatrix} - \varepsilon\ell \begin{bmatrix} \cos\varphi_1 \\ \cos\varphi_2 \end{bmatrix} - \alpha\ell \begin{bmatrix} \sin\varphi_1 \\ \sin\varphi_2 \end{bmatrix} \right) = 0, \tag{39}$$

that can be solved to get the correction $\boldsymbol{q}^c_{i+1,j+1}$.

4. Numerical results

In this section, results of numerical simulations are presented to provide an insight into the characteristic deformation mechanisms of the discrete duoskelion beam model introduced above. More particu larly, studies are performed for different numbers N_c of periodically repeated cells and for different constraints and loads. Three cases are examined for what concerns constraints, namely (*a*) simply sup ported, (*b*) clamp sliding support, and (*c*) cantilever conditions. For what concerns applied loads, (*a*) traction, (emphb) compression, and (*c*) mixed traction shearing conditions are considered at the right extremal midpoint (*i.e.* point B in Fig. 3) of the duoskelion beam.

Additionally, simulations are performed to assess the influence of geometry imperfections, and suitable load perturbations are exploited to find different deformed configurations for the same applied load in the large displacement regime. Each analysis is carried out for an increasing number of periodically repeated cells, *i.e.* $N_c = 20,\ 40,\ 80$, while keeping fixed the total duoskelion beam length and the aspect ratio of periodically repeated cells. As the quantity N_c is increasing, the following asymptotic scaling is applied to the *finite* stiffnesses k_a and k_b

$$\begin{aligned} k_a &\approx N_c, \\ k_b &\approx N_c^{-1}. \end{aligned} \tag{40}$$

According to the scaling above, the ratio k_a/k_b between the finite exten sional and bending stiffness behaves asymptotically as N_c^2. The question that is here investigated is whether and in which conditions the family of discrete duoskelion beams introduced above, parametrized over the number of periodically repeated cells N_c and fulfilling the scaling in Eq. (40), exhibits a mechanical behavior converging to a limit one, *i.e.* more and more unaffected by increasing N_c.

Having in mind the objective above, aimed at keeping consistency in analyzing numerical simulations performed for different periodically repeated cell numbers, when not specified otherwise simulations are terminated when the same displacement of the right extremal midpoint,

[4] Indeed, with an abuse of notation, it is considered that $\boldsymbol{q}_i = (\varphi_1, \varphi_2)$, $\boldsymbol{q}^c_{i+1,j+1} = (\varphi_1^c, \varphi_2^c)$, and $\Delta\boldsymbol{q}_{i+1,j} = (\Delta\varphi_1, \Delta\varphi_2)$.

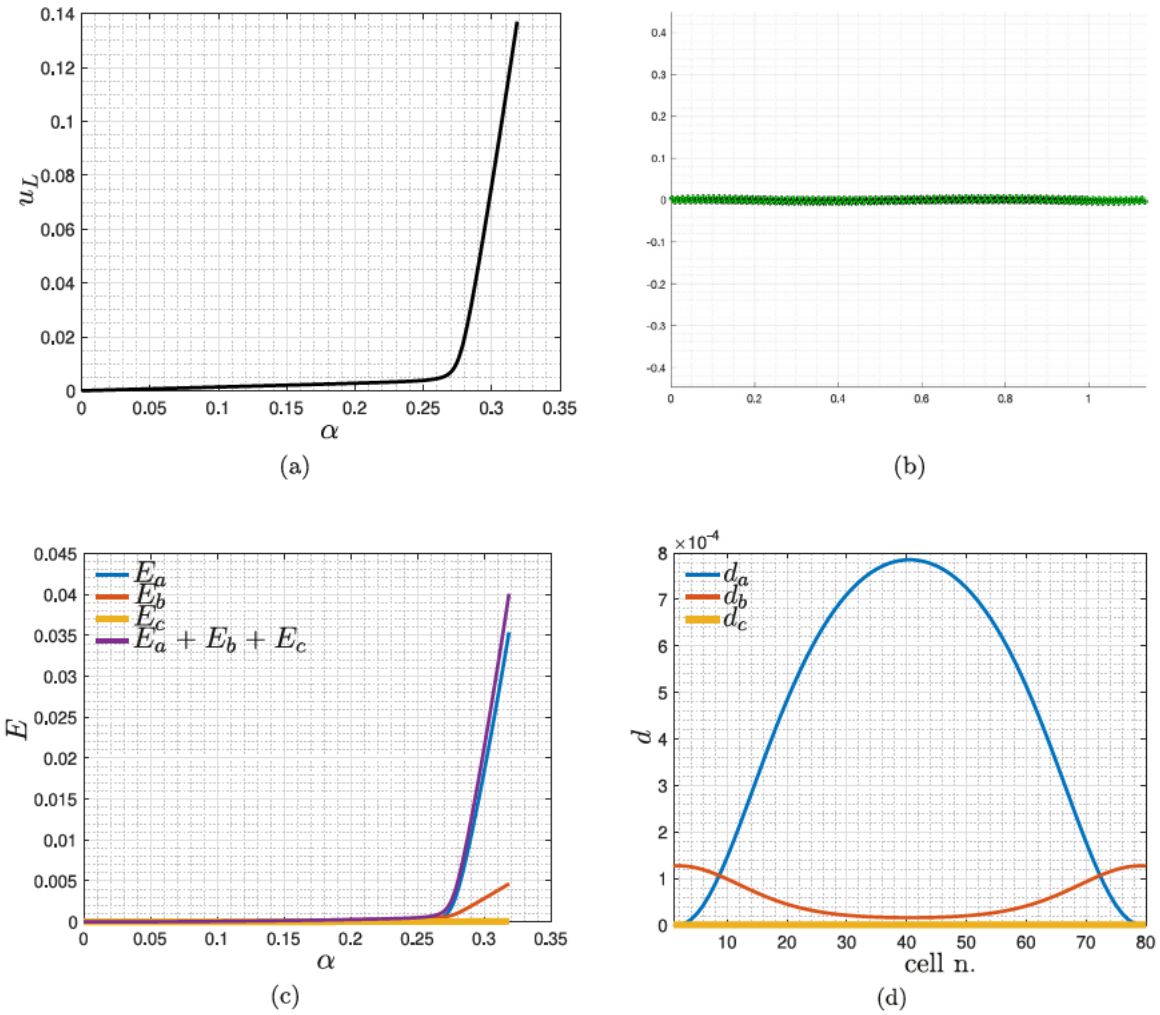

Fig. 14. Duoskelion beam formed by 80 cells subjected to clamp-sliding support kinematic conditions and traction force: equilibrium path (a), final deformation (b), energy evolution (c) and cell energy density (d).

i.e. the midpoint where the external load is applied, is reached in the computational process described in the previous section.

According to the scaling above, the finite extensional stiffness is increasing with N_c. Aimed at ensuring the comparison among results obtained for different N_c's to be consistent, once chosen stiffnesses' values for the lowest cell number, the ratio among the extensional $\ll$ infinite $\gg$ stiffness and the finite one is kept constant with N_c, as well as the ratio among the shearing stiffness and the finite extensional one. As, according to the scaling above, the finite bending stiffness is decreasing with N_c, then the value of $\ll$ infinite $\gg$ bending stiffness can be kept constant.

Recall that this work aims at presenting results of a numerical study performed to understand the qualitative deformation patterns and mechanisms of duoskelion beams. For such a study only the ratio between specific quantities is relevant, not really the values of parame ters and other defined quantities. Therefore, henceforth, all parameters (both constitutive and geometric) and quantities will be assumed as expressed in the International System's units of measure. Numerical values for parameters used in computations are provided in Tables 1 (stiffnesses) and 2.

Table 1
Stiffnesses' values used for parameters in simulations for $N_c = 20$ only. For any other N_c, $\ll$ finite $\gg$ stiffness parameters can be retrieved via the scaling law, while $\ll$ infinite $\gg$ ones can be retrieved according to the discussion on ratios between stiffnesses.

	k_a	k_b	k_c
kind	N/m	N m	N/m
infinite	10^8	10^2	10^8
finite	10^3	10^{-3}	–

Table 2
Numerical values used for parameters in simulations.

L	η	e
m	–	–
1	10^{-8}	5

4.1. Simply supported duoskelion beam subjected to traction force

In this subsection, simply supported kinematic conditions are taken into account for the duoskelion beam. Namely, the left extremal mid point (*i.e.* point A in Fig. 3) of the duoskelion beam is hinged, so to remain fixed while allowing for rigid rotations of the whole system. The right extremal midpoint of the duoskelion beam is constrained to move only along the beam axis, *i.e.* horizontally. Thus, any rigid motion of the whole system is avoided. A traction force, *i.e.* axial and toward the outward direction, with magnitude α is applied to the right extremal midpoint.

Fig. 6(a) reports on the equilibrium path of the simply supported duoskelion beam subjected to traction force for $N_c = 20$. Fig. 6(b) shows the deformed shape of the duoskelion beam with $N_c = 20$ for

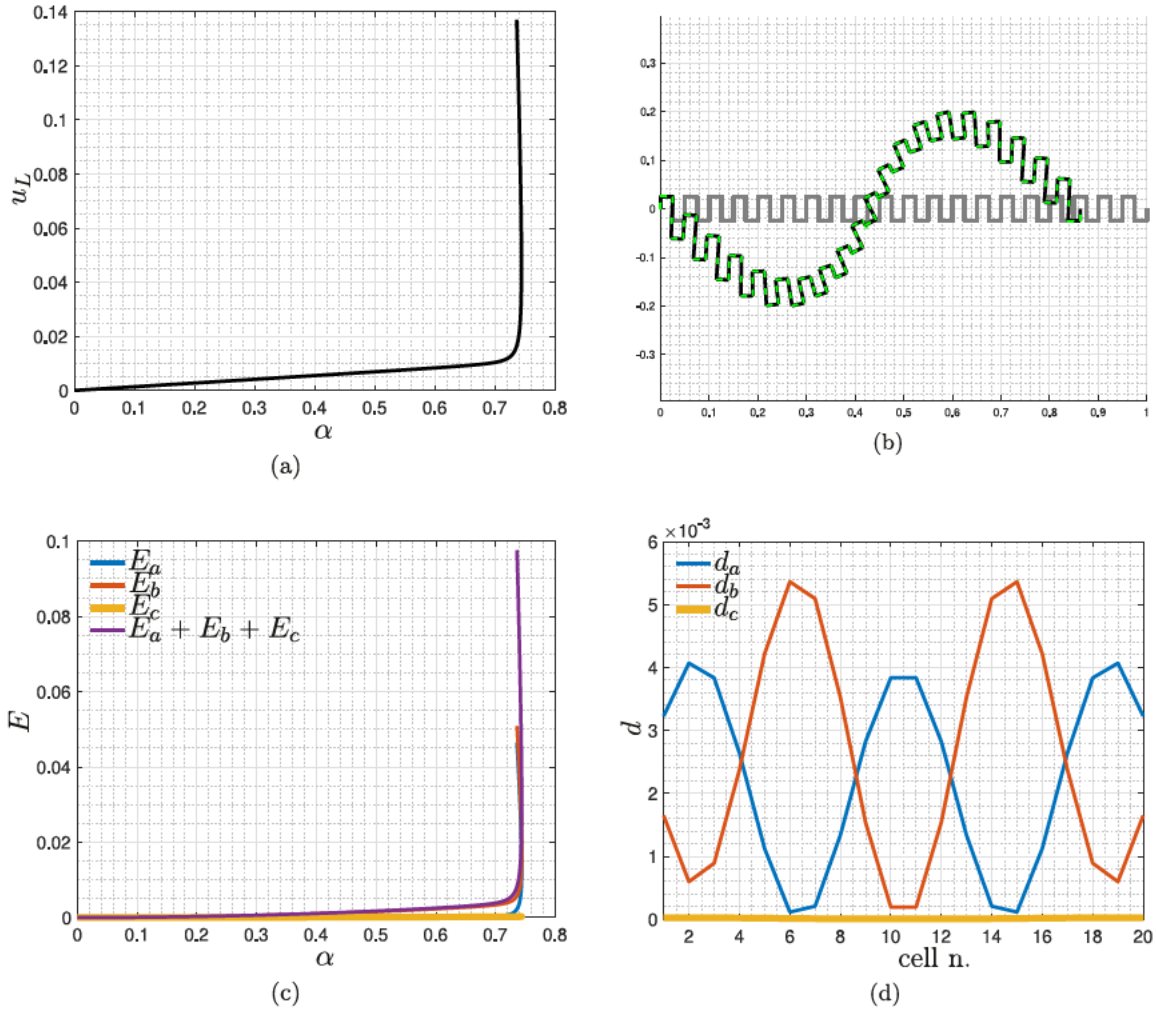

Fig. 15. Duoskelion beam formed by 20 cells subjected to clamp-sliding support kinematic conditions and compression force: equilibrium path (a), final deformation (b), energy evolution (c) and cell energy density (d).

the last converged step. Fig. 6(c) accounts for the total deformation energy E^{def} ($E_a + E_b + E_c$) of the duoskelion beam with $N_c = 20$ along the sequence of converged equilibrium steps. In the same plot, such a total deformation energy is decomposed in its different addends, *i.e.* total extensional (E_a), bending (E_b), and shearing (E_c) energies. Finally, for the last converged solution and $N_c = 20$, Fig. 6(d) shows on the ordinate the contributions to the deformation energy, *i.e.* extensional (d_a), bending (d_b), and shearing (d_c) one, for each periodically repeated cell (in the abscissa). In other words, for each periodically repeated cell (indexed with increasing numbers from the left to the right), all elementary homologous contributions are summed up to give Fig. 6(d). This plot thus gives for each periodically repeated cell a kind of global indication of its energy level. Having in mind the idea of representing the duoskelion beam, say the set of its midpoints, with a one dimensional continuum embedded in the plane, Fig. 6(d) would give the energy density of such a continuum.

Figs. 7(a, b, c, d) and 8(a, b, c, d) are analogous to Fig. 6(a, b, c, d), but are referred to $N_c = 40$ and $N_c = 80$, respectively. According to the definition given in the previous section, the equilibrium path is, strictly speaking, a one dimensional curve embedded in a real space with dimensions equal to $N + 1$. Aimed at giving a two dimensional representation of the equilibrium path, Figs. 6(a), 7(a), and 8(a) plot the couple formed by the absolute value of the horizontal, *i.e. axial* with respect to the whole beam, displacement u_L of the right extremal midpoint and the quantity α for each equilibrium step computed by the algorithm.

When not specified otherwise, the algorithm is initialized at the trivial equilibrium point given by the undeformed configuration and $\alpha_0 = 0$. The equilibrium curves in Figs. 6(a), 7(a), and 8(a) are then computed progressively. It is worth to notice that the *two dimensional* equilibrium paths in Figs. 6(a), 7(a), and 8(a) can actually be regarded as plots of the quantity u_L as a function of the magnitude α of the applied load. In Figs. 6(a), 7(a), and 8(a) it is seen that, for all numbers of periodically repeated cells, the quantity u_L is almost insensitive to the increment of loading magnitude, until a threshold for the quantity α is not reached starting from $\alpha = 0$. Such a threshold appears to be independent of N_c. Afterwards, a kind of linear, yet very stiff, behavior is observed for u_L when increasing α, which seems also independent of N_c. Remark that no buckling/bifurcation phenomenon is occurring for α being equal to the threshold value. Indeed, for the whole computation, the stiffness matrix $\frac{\partial^2 E^{\text{def}}}{\partial \mathbf{q} \partial \mathbf{q}}$ is positive definite, thus also indicating that the analyzed equilibrium path is a stable one, *i.e.* made up of stable equilibrium points. The form of the equilibrium paths in Figs. 6(a), 7(a), and 8(a) suggests that duoskelion beams might be exploited as switches sensible to extensional stimuli.

In Figs. 6(b), 7(b), and 8(b), oriented green segments in the deformed configuration stemming from nodes point toward the direction of unit arrows attached to them, while black segments indicate links. The initial reference configuration is colored in gray. Figs. 6(b), 7(b), and 8(b) show that, for all considered N_c's, the midpoints of the duoskelion beam remain aligned and arrange along the direction of

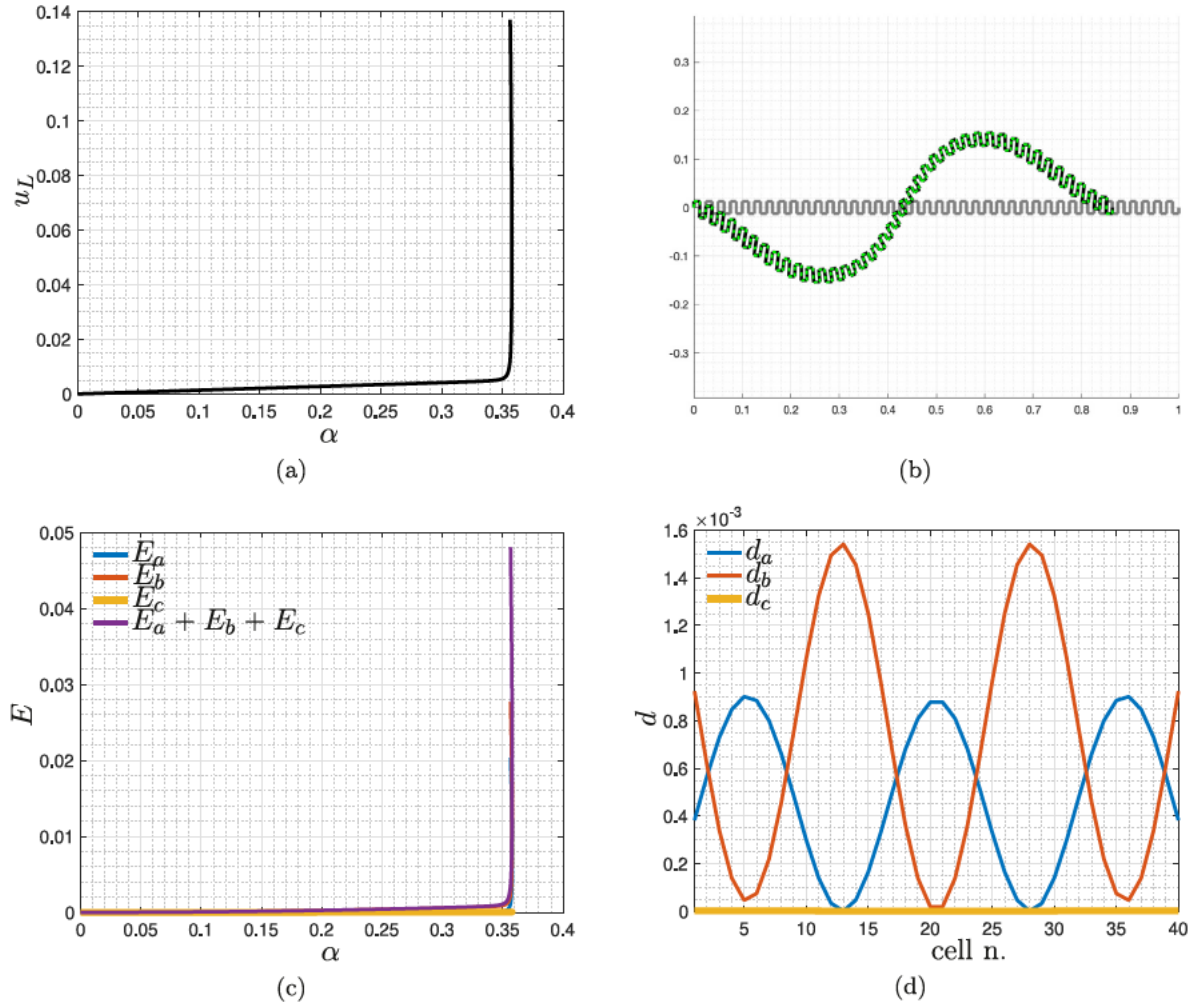

Fig. 16. Duoskelion beam formed by 40 cells subjected to clamp-sliding support kinematic conditions and compression force: equilibrium path (a), final deformation (b), energy evolution (c) and cell energy density (d).

the applied load, which incidentally is the initial one. It is worth to remark that the duoskelion beam clearly shows some characteristic symmetry properties that play a role in its overall behavior. Indeed, while the geometry of the undeformed duoskelion beam is invariant upon $\pm 180°$ rotations, it is not as such when reflected with respect to its axial (x) and transverse (y) axes (see Fig. 3). This is the reason why the duoskelion beam is considered to be a *chiral* structure. Clearly, beams with *opposite* chirality, obtainable one from the other by reflection, might be considered. Opposite chiralities obviously affect differently the overall behavior of the beam, being the different results relatable by specific symmetries.

Looking at Figs. 6(b), 7(b), and 8(b) it is observed that all period ically repeated cells deform equally. Indeed, looking at the midpoints, a homogeneous elongation is observed. Such an elongation is due to the rotation of the rigid(ified) two legged bodies and to the elonga tion of the links with finite extensional stiffness. This characteristic deformation mechanism thus consists in the rigid two legged bodies rotating anti clockwise, all of the same angle, and links with finite extensional stiffness elongating all of the same amount. Clearly, the rotation direction of the rigid two legged bodies is determined by the chirality of the structure. Remark that two adjacent, *i.e.* having a common node, links with finite extensional stiffness undergo the same elongation/compression because the bending stiffness controlling their relative angle is considered as *infinite* according to the ratios between stiffnesses discussed above. Therefore, they behave as a unique truss.

Previous considerations, based on the deformation pattern, claiming that only links with finite extensional stiffness were deforming are cor roborated by Figs. 6(c, d), 7(c, d), and 8(c, d). Indeed, Figs. 6(c), 7(c), and 8(c) show that, roughly speaking, the only non zero deformation energy, which thus accounts for the whole total energy, is the one stored in extension of links. It is worth to remark that shearing energy is negligible with respect to both extensional and bending energies. In addition, based on the deformation pattern, claiming that all cells deform equally are confirmed by Figs. 6(d), 7(d), and 8(d), as all energy contributions, *i.e.* extensional, bending and shearing, for each cell are constant along the beam.

It is finally worth remarking that, when different finite stiffnesses scalings are considered, the characteristic behavior of the duoskelion beam in the simply supported traction test is expected to remain unchanged. Indeed, in such a test the deformation mechanism does not involve bending deformation of Timoshenko like elements, notwith standing that according to the applied scaling extensional resistance is asymptotically greater than the bending one with increasing N_c.

4.2. *Simply supported duoskelion beam subjected to compression force*

In this subsection, simply supported kinematic conditions are taken into account for the duoskelion beam. A compression force, *i.e.* axial and toward the inward direction, with magnitude α is applied to the right extremal midpoint.

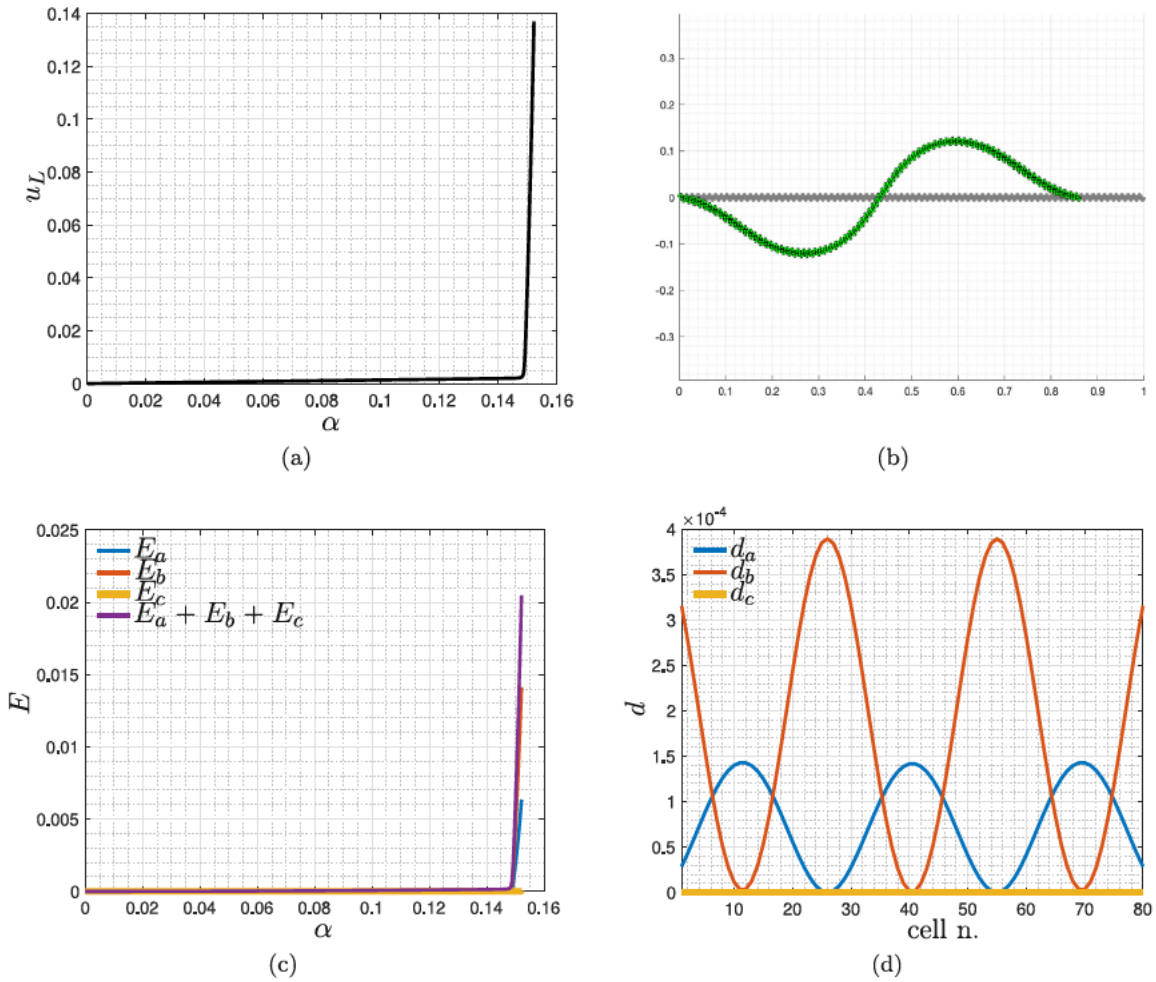

Fig. 17. Duoskelion beam formed by 80 cells subjected to clamp-sliding support kinematic conditions and compression force: equilibrium path (a), final deformation (b), energy evolution (c) and cell energy density (d).

Fig. 9(a) reports on the equilibrium path of the simply supported duoskelion beam, formed by $N_c = 20$ periodically repeated cells, subjected to compression force. Fig. 9(b) shows the shape of the duoskelion beam for the last converged step, being $N_c = 20$. Fig. 9(c) accounts for deformation energies stored within the duoskelion beam ($N_c = 20$) along the sequence of converged equilibrium steps. Finally, for the last converged solution and $N_c = 20$, Fig. 9(d) shows contributions to the total deformation energy, *i.e.* extensional (d_a), bending (d_b), and shearing (d_c), for each periodically repeated cell. Figs. 10(a, b, c, d) and 11(a, b, c, d) are analogous to Fig. 9(a, b, c, d), but are referred to $N_c = 40$ and $N_c = 80$, respectively.

In Fig. 9(a) a quasi linear force displacement relationship is observed, which is seemingly unaffected by changes in N_c. Remark that no buckling/bifurcation phenomenon is occurring throughout the whole computation. Indeed the stiffness matrix is positive definite for the whole equilibrium path, thus indicating also that it is made up of stable equilibrium points.

Figs. 9(b), 10(b), and 11(b) show, as in the previous traction case, that for all N_c's the midpoints of the duoskelion beam remain aligned and arrange along the direction of the applied load, which incidentally is the initial one. Looking at Figs. 6(b), 7(b), and 8(b) it is observed that, as for the previous traction case, all periodically repeated cells deform equally. In other words, a homogeneous compression is observed when looking at midpoints, being such a compression due to the rotation of the rigid two legged bodies and to the bending of Timoshenko like elements with finite bending stiffness. This characteristic deformation mechanism thus consists in the rigid two legged bodies rotating anti clockwise all of the same angle and Timoshenko like elements with finite bending stiffness all inflecting of the same amount. Clearly, also in this case the rotation direction of the rigid two legged bodies is determined by the chirality of the structure.

Previous considerations claiming that only Timoshenko like elements with finite bending stiffness are deforming can be corroborated by Figs. 9(c, d), 10(c, d), and 11(c, d). Indeed, Figs. 9(c), 10(c), and 11(c) show that, roughly speaking, the only non zero deformation energy, which thus accounts for the whole total energy, is the bending one. It is worth to remark that shearing energy is greater than, and thus non negligible with respect to, extensional energy. Therefore, it is observed *a posteriori* that the hypothesis of shearing undeformability introduced above is not respected for the choice made for the stiffnesses value. Nevertheless, results are deemed reliable as both extensional and shearing energies are negligible with respect to bending energy.

The fact that all cells deform equally is confirmed by Figs. 9(d), 10(d), and 11(d), as all energy contributions are constant with the cells. Furthermore, it is expected that, considering different finite stiffnesses scalings such that $k_a/k_b \approx N_c^h$, with $h \leq 1$, *i.e.* implying the Timoshenko like elements with finite bending stiffness to be asymptotically less deformable in bending, could lead to a dramatic change in the behavior of the duoskelion beam in the simply supported compression test. Indeed, as in such a test only Timoshenko like elements with finite bending stiffness are deforming, these different scalings could lead, in

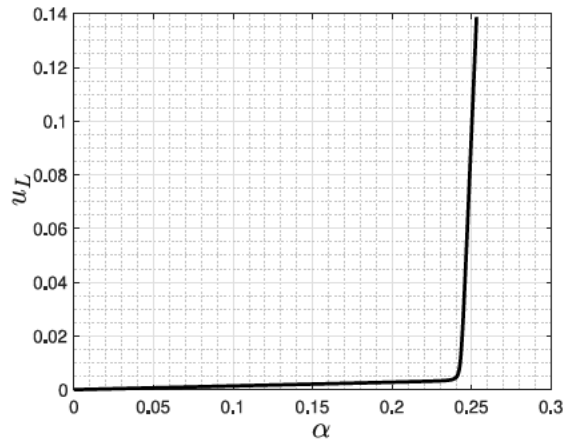

(a)

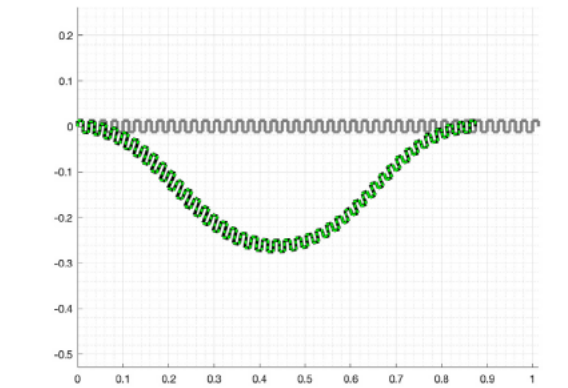

(b)

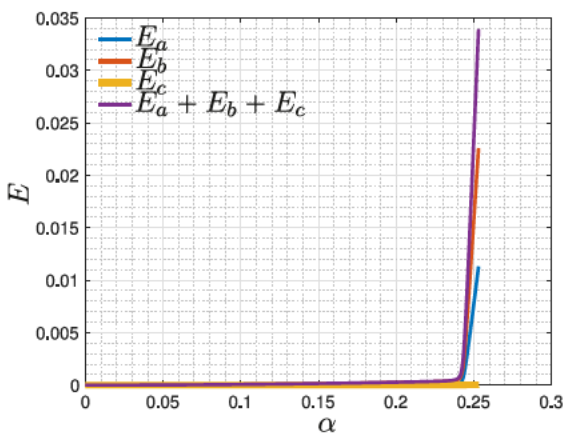

(c)

Fig. 18. Duoskelion beam formed by 40.5 cells subjected to clamp-sliding support kinematic conditions and compression force: equilibrium path (a), final deformation (b), energy evolution (c).

the limit of $N_c \to \infty$, to a system which behaves, as a whole, like an incompressible beam.

4.3. Clamp sliding support kinematic conditions and traction force

In this subsection, clamp sliding support kinematic conditions are taken into account for the duoskelion beam. Namely, the left extremal midpoint of the duoskelion beam is hinged so to remain fixed, and the rotation of the corresponding link is enforced to be zero.[5] Thus, any rigid motion of the whole system is avoided. The right extremal midpoint of the duoskelion beam is constrained to move only along the beam axis, *i.e.* horizontally, and the rotation of the corresponding link is enforced to be zero as well. A traction force, *i.e.* axial and toward the outward direction, with magnitude α is applied to the right extremal midpoint.

It is worth to remark that the results of this sub section are partially relatable and in agreement with those experimentally found in [38] for a fixed number of periodically repeated cells and for a physical system whose proper modeling would nevertheless require, within the approach presented here, a different choice for ratios between homologous and non homologous stiffnesses.

Figs. 12(a) reports on the equilibrium path of the duoskelion beam subjected to clamp sliding support kinematic conditions and traction force, being $N_c = 20$. Fig. 12(b) shows the shape of the duoskelion beam for the last converged step and for $N_c = 20$. Fig. 12(c) accounts for deformation energies stored within the duoskelion beam ($N_c = 20$) along the sequence of converged equilibrium steps. Finally, Fig. 12(d) shows, for the last converged solution and $N_c = 20$, the contributions to the deformation energy, *i.e.* extensional (d_a), bending (d_b), and shearing (d_c) one, for each periodically repeated cell. Figs. 13(a, b, c, d) and 14(a, b, c, d) are analogous to Fig. 12(a, b, c, d), but are referred to $N_c = 40$ and $N_c = 80$, respectively.

In Figs. 12(a), 13(a), and 14(a) it is seen that, for all numbers of periodically repeated cells, the quantity u_L is almost insensitive, yet seemingly depending linearly, on the loading magnitude α, until a threshold for α is reached. The slope of such a line decreases with N_c. The threshold for α appears to be decreasing with the number of periodically repeated cells. Beyond such a threshold, u_L behaves seemingly linearly when increasing α, with a slope which appears to be decreasing with N_c. Remark that, also in this case, no buck ling/bifurcation phenomenon is occurring for α being equal to the threshold value. Indeed, for the whole computation, the stiffness matrix is positive definite, thus also indicating that the analyzed equilibrium paths are stable ones.

Figs. 12(b), 13(b), and 14(b) deserve a thorough description. In deed, being rotations of the two extremal links fixed to be zero, the homogeneous configuration[6] obtained for the simply supported beam is no more kinematically admissible. Therefore, the system minimizes its energy according to the applied constraints and loading by assuming a configuration showing (*a*) non homogeneous extension of links with finite extensional stiffness, (*b*) non homogeneous rotation of two legged rigid bodies, and (*c*) midpoints forming a S shaped line which is symmetric with respect to the transverse axis (y) in Fig. 3.

Clearly, also in this case the rotation direction of the rigid two legged bodies is determined by the chirality of the structure. It also straightforward to see that the concavity of the S shaped line formed by midpoints is linked to the chirality of the beam. Indeed, a solution with midpoints forming the same S shape but with opposite concav ity, for the same deformation energy and applied kinematic/loading conditions, cannot be obtained by applying a rotation of $\pm 180°$ to the deformed configuration. Such a solution can be obtained only by applying a reflection with respect to the axial (x) or transverse (y) axes in Fig. 3, namely by considering a beam with the opposite chirality. At the continuum scale, such a S shape formed by the midpoints would imply a coupling, induced by the non symmetry (chirality) of the structure, between flexure and extension (see [47].

[5] Actually, it is the rotation of the left extremal joint that is enforced to be zero. Nevertheless, recalling that the shearing stiffness is considered to be infinite, it can be equivalently stated that the rotation of the link adjacent to the left extremal midpoint is enforced to be zero.

[6] Indeed less energetic in terms of total energy for the same applied load/displacement and N_c, since it is obtained as optimum solution to a less constrained problem.

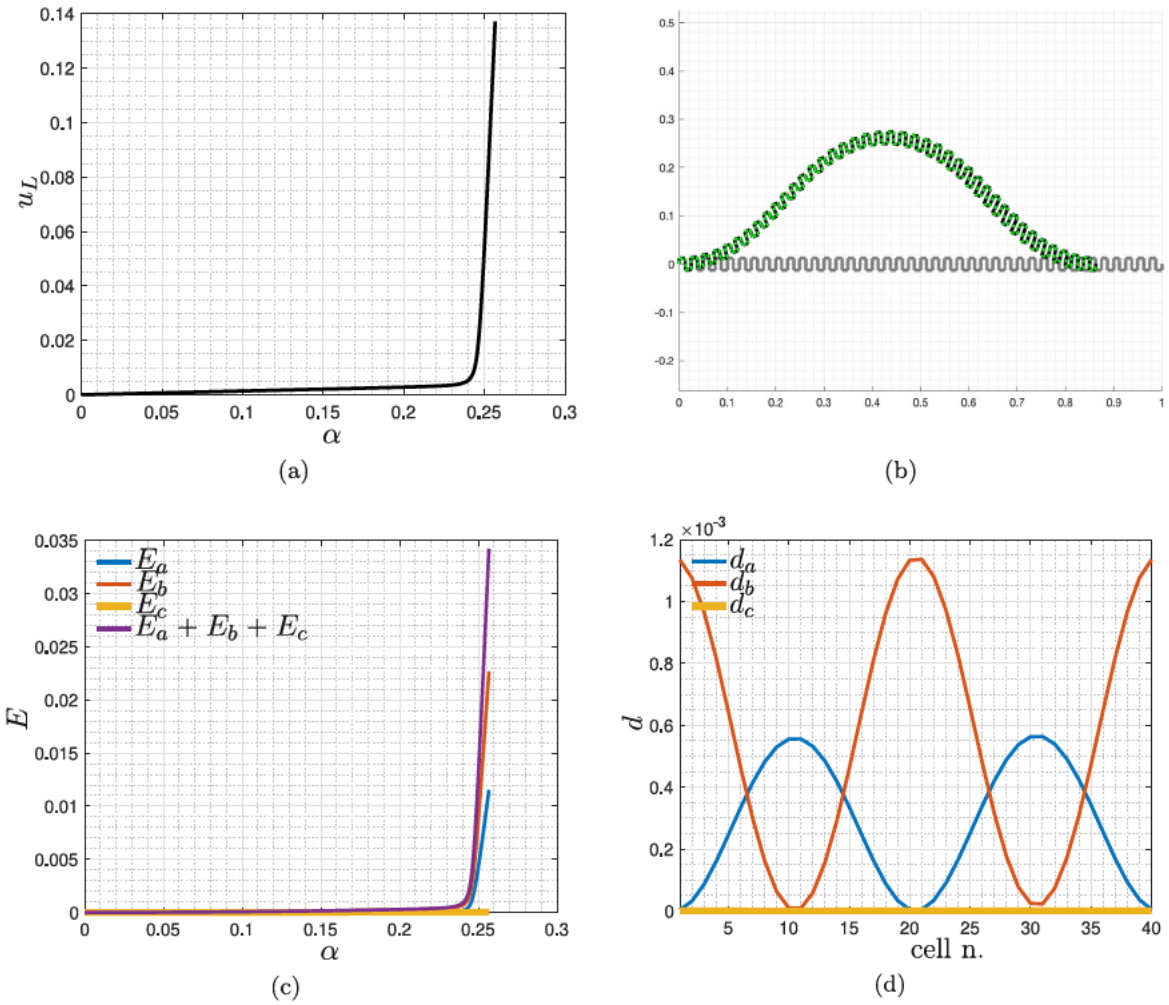

Fig. 19. Duoskelion beam formed by 40 cells subjected to clamp-sliding support kinematic conditions, compression force at the right end-point and modulated transverse perturbation load directed upward at the central midpoint: equilibrium path (a), final deformation (b), energy evolution (c) and cell energy density (d).

Remark that, for the adopted asymptotic scaling of finite stiffnesses, in this test the amplitude of the S shaped line formed by the midpoints seems to vanish for $N_c \to \infty$. Indeed, for $N_c \to \infty$ the duoskelion beam seems to approach a straight configuration, and particularly one which resembles that obtained for the simply supported beam. This evidence suggests that, for these scaling and external applied conditions, the effect of kinematic conditions on the rotation of extremal links is vanishing for the number of periodically repeated cells going to infinite. The rotation angles of the two legged rigid bodies and the extension of links with finite extensional stiffness are homogeneous in the bulk of the system and are varying within a transition zone at boundaries of the duoskelion beam. Such a zone is progressively reduced as N_c approaches infinity and eventually vanishes.

Remark that, while the amplitude of the S shape formed by mid points is decreasing and eventually vanishing for $N_c \to \infty$, such a S shape actually assumes its maximum and minimum points at different positions in space for increasing N_c, eventually turning into multiple concatenated S shapes. It is reasonable to conjecture that such a process could lead to a mid line with increasingly many smooth zig zag's having a vanishing amplitude, *i.e.* a straight line.

Figs. 12(c), 13(c), and 14(c) show that extensional energy is increasingly relevant for increasing N_c and, eventually, *i.e.* in the limit $N_c \to \infty$, it accounts for the whole deformation energy of the system. Figs. 12(d), 13(d), and 14(d) show that, not only the ratio between extensional energy and bending energy is increasing with N_c, but also that extensional energy is more relevant in the middle of the specimen, while bending energy is more relevant in proximity of the system's left and right boundaries.

4.4. Clamp sliding support kinematic conditions and compression force

In this subsection, clamp sliding support kinematic conditions are considered for the duoskelion beam. A compression force, *i.e.* axial and toward the inward direction, with magnitude α is applied to the left extremal midpoint.

Fig. 15(a) reports on the equilibrium path of the duoskelion beam subjected to clamp sliding support kinematic conditions and traction force, being $N_c = 20$. Fig. 15(b) shows the shape of the duoskelion beam with $N_c = 20$ for the last converged step. Fig. 15(c) accounts for deformation energies stored within the duoskelion beam ($N_c = 20$) along the sequence of converged equilibrium steps. Finally, for the last converged solution, Fig. 15(d) shows the contributions to the deformation energy, *i.e.* extensional (d_a), bending (d_b), and shearing (d_c) one, for each periodically repeated cell. Figs. 16(a, b, c, d) and 17(a, b, c, d) are analogous to Fig. 15(a, b, c, d), but are referred to $N_c = 40$ and $N_c = 80$, respectively.

In Figs. 12(a), 13(a), and 14(a) it is seen that, for all numbers of periodically repeated cells, the quantity u_L is almost insensitive, yet behaving linearly, on the loading magnitude α, until a threshold for α is reached. The slope of such a line decreases with N_c. The threshold for α appears to be decreasing with the number of periodically repeated cells. Following such a threshold, a kind of ≪ weak ≫ snap back is observed,

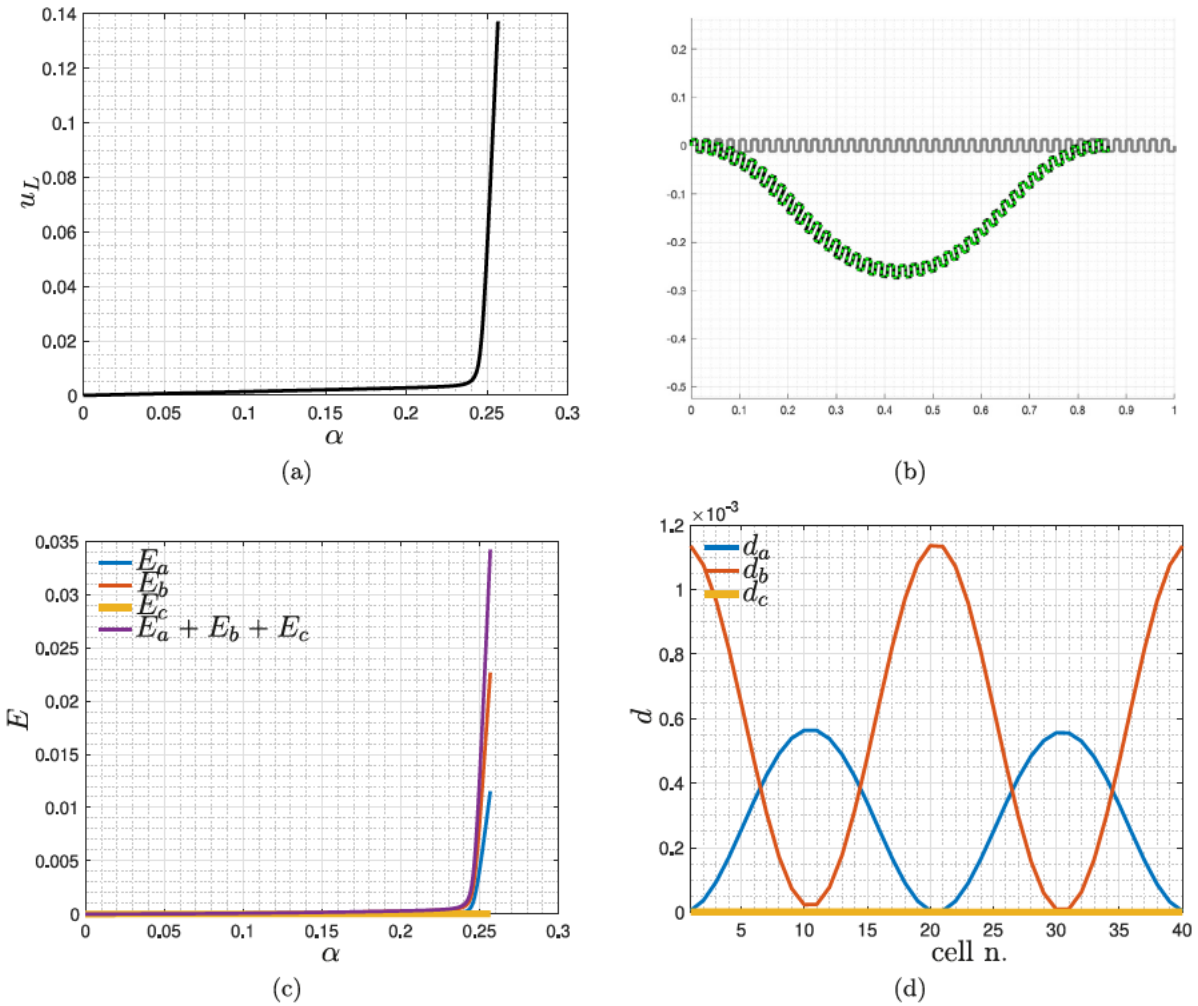

Fig. 20. Duoskelion beam formed by 40 cells subjected to clamp-sliding support kinematic conditions, compression force at the right end-point and modulated transverse perturbation load directed downward at the central midpoint: equilibrium path (a), final deformation (b), energy evolution (c) and cell energy density (d).

thus not being possible to express u_L as a function of α. Remark that, also in this case, no buckling/bifurcation phenomenon is occurring for α being equal to the threshold value. Indeed, for the whole computation, the stiffness matrix is positive definite.

Figs. 12(b), 13(b), and 14(b) show that the system minimizes the to tal energy according to the applied constraints and loading by assuming a configuration with (a) non homogeneous extension of links with finite extensional stiffness, (b) non homogeneous rotation of two legged rigid bodies, and (c) midpoints forming a S shape which is symmetric with respect to the transverse axis (y) in Fig. 3. Clearly, the rotation direction of the rigid two legged bodies is also determined. also in this case, by the chirality of the structure and, by the same argument employed for the previous test, it is straightforward to check that the concavity of the S shape formed by midpoints is linked to the chirality of the beam.

Remark that, differently from the previous test, for the adopted asymptotic scaling of finite stiffnesses, in this test the amplitude of the S shape is very relevant with respect to the length of the beam and seems to decrease less and less for increasing N_c, suggesting that such a shape might be kept $\ll$ finite $\gg$ in the limit of $N_c \to \infty$. The rotation angles of the two legged rigid bodies and the extension of links with finite extensional stiffness are varying throughout the beam axis: elongation occurs in proximity of the boundaries and compression occurs in the bulk. Remark that the S shape formed by midpoints assumes its maximum and minimum points at the same spatial positions along the beam axis when increasing N_c.

Figs. 12(c), 16(c), and 17(c) show that bending energy is increas ingly relevant for increasing N_c and, eventually, *i.e.* in the limit $N_c \to \infty$, it is expected to account for the whole deformation energy of the system. Figs. 15(d), 16(d), and 17(d) show that, not only the ratio between extensional and bending energy is decreasing with N_c, but also that extensional and bending energies have a periodic sinusoidal behavior with opposite phases.

At this point, the analysis will be directed toward understanding how a small geometrical imperfection in the microstructure, such that it cannot be taken into account in the homogenized modeling, affects the behavior of the system. To this aim the structure ($N_c = 40$), while keeping its chirality, has been symmetrized with respect to the transverse (y) axis in Fig. 3 by adding half periodically repeated cell rightmost the duoskelion beam (see the gray undeformed con figuration in Fig. 18(b)). Such a geometrical imperfection has a size behaving asymptotically like $1/N_c$. Therefore, it should be invisible to the homogenization process. Remark that, while the geometry of the undeformed duoskelion beam is now symmetric with respect to the transverse axis of the beam, mechanical interactions are not because of the hypotheses made above on the ratios between homologous and non homologous stiffnesses. Indeed, the left extremal link belongs to a rigid two legged body, while the right extremal link has a finite extensional stiffness. Thus, kinematic conditions are applied to two extremal parts behaving differently mechanically.

It is seen by Fig. 18(a) that the equilibrium path changes qualita tively only beyond the threshold value for α. The equilibrium path does

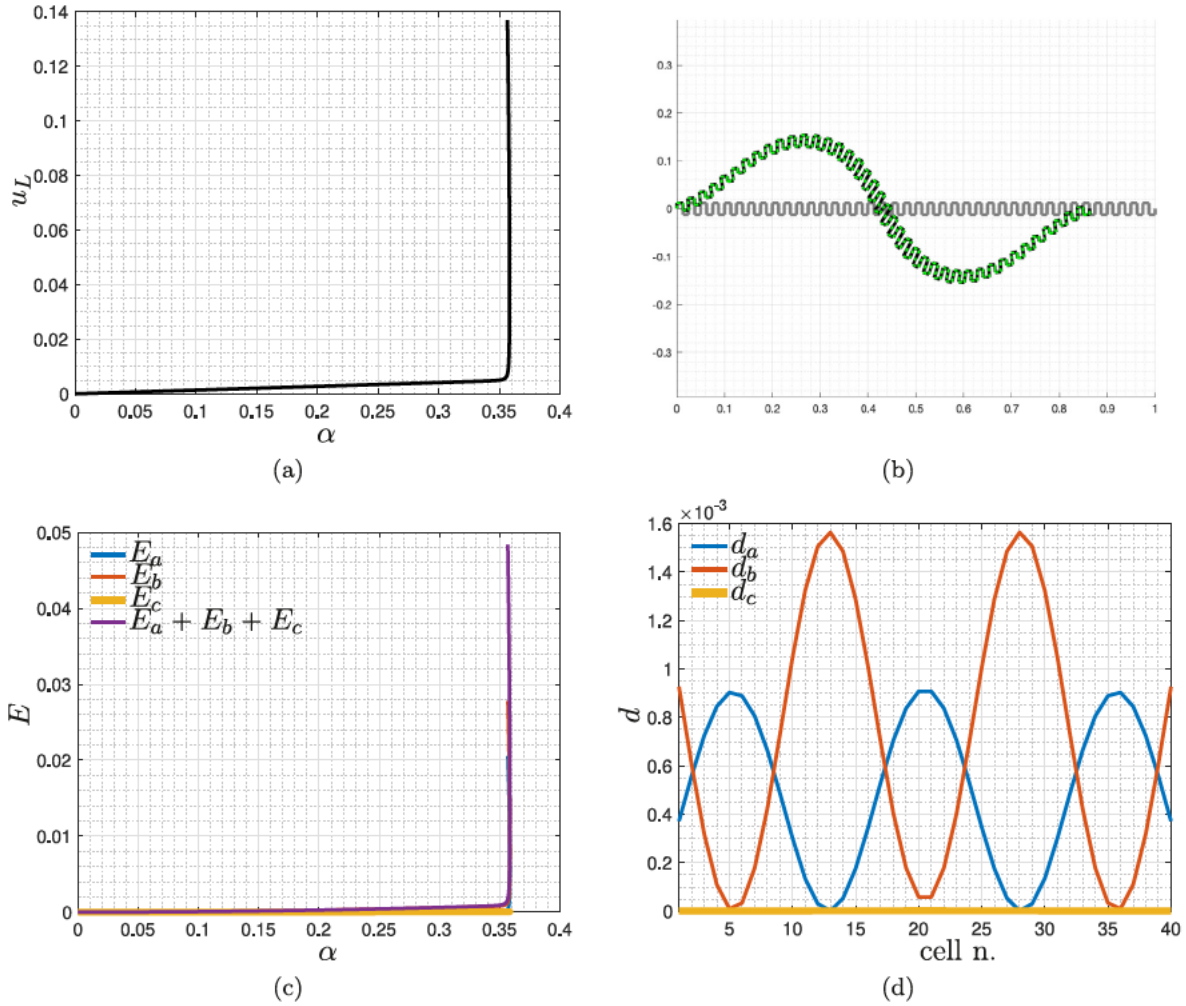

Fig. 21. Duoskelion beam formed by 40 cells subjected to clamp-sliding support kinematic conditions, compression force at the right end-point and modulated transverse perturbation loads at (from the left to the right) 1/4 and 3/4 of the total beam length directed, respectively, upward and downward: equilibrium path (a), final deformation (b), energy evolution (c) and cell energy density (d).

not exhibit any more a snap back. Fig. 18(b) shows that the deformed shape of the beam is dramatically changed. Indeed, the geometrical imperfection induces very large (with respect to the total length of the duoskelion beam) midpoints' displacements in the transverse direction that do not form any more a S shape but, rather, a bell shape. It is interesting to notice that links with finite extensional stiffness are elongated in the left half of the beam and compressed in the right half of it.

It is now to be investigated whether there exist multiple equilibrium configurations corresponding to the same compression load. To this aim, a modulated transverse perturbation is applied to the central mid point of the beam ($N_c = 40$). Results are reported in Figs. 19 (upward perturbation) and 20 (downward perturbation). Such a perturbation has a magnitude which is very small compared to the maximum com pression load reached during the algorithm run. For each perturbation direction, two consecutive algorithm runs are actually employed. In the first run, the external loading is given by a perturbation, independent of α, in the transverse direction and by a traction force which is proportional to α. Starting from the final equilibrium configuration found by this first algorithm run,[7] a second algorithm run is executed. In such a second run, the transverse load has a magnitude $(\alpha_{f1} - \alpha_{f0}) - \alpha$, *i.e.* decreasing with α and eventually vanishing for $\alpha = \alpha_{f1} - \alpha_{f0}$, and the traction load has a magnitude $\alpha + \alpha_{f0}$. When, during the second algorithm run, the quantity $\alpha + \alpha_{f0}$ is equal to α_{f1}, then the computation is stopped. An equilibrium configuration which is different from that reported in Fig. 16 is obtained such that, nonetheless, the applied loads and kinematic conditions are the same.

Remark that, incidentally, the displacement u_L of the right tip seems to be for the last step of both Figs. 19 and 20 very close to that in Fig. 16, while being only the compression force, strictly speaking, the same. Note that in Fig. 19 links with finite extensional stiffness are elongated in the right half of the system and compressed in the left half. It is additionally noted that Figs. 19 and 20 are indeed showing the same experiment, since one can be obtained from the other by applying a $\pm 180°$ rotation.

An analogous analysis has been carried out applying two (equal and opposite) modulated transverse perturbations to midpoints at, respec tively, 1/4 and 3/4 of the total beam length to obtain two opposite (in concavity) S shaped deformed configurations. Results are reported in Figs. 21 and 22. It is noted that the two deformed shapes in Figs. 21 and 22 cannot be obtained one from the other through a rotation, not only because midpoints form S shapes with different concavities and two legged bodies rotate in opposite directions, but also because in Fig. 21 links with finite extensional stiffness are elongated in the bulk of the beam and compressed at boundaries, while the opposite behavior is observed in Fig. 21.

[7] The first algorithm run is stopped for a value of α (say α_{f0}) less than the one (say α_{f1}) obtained in the last step of the computation reported in Fig. 16.

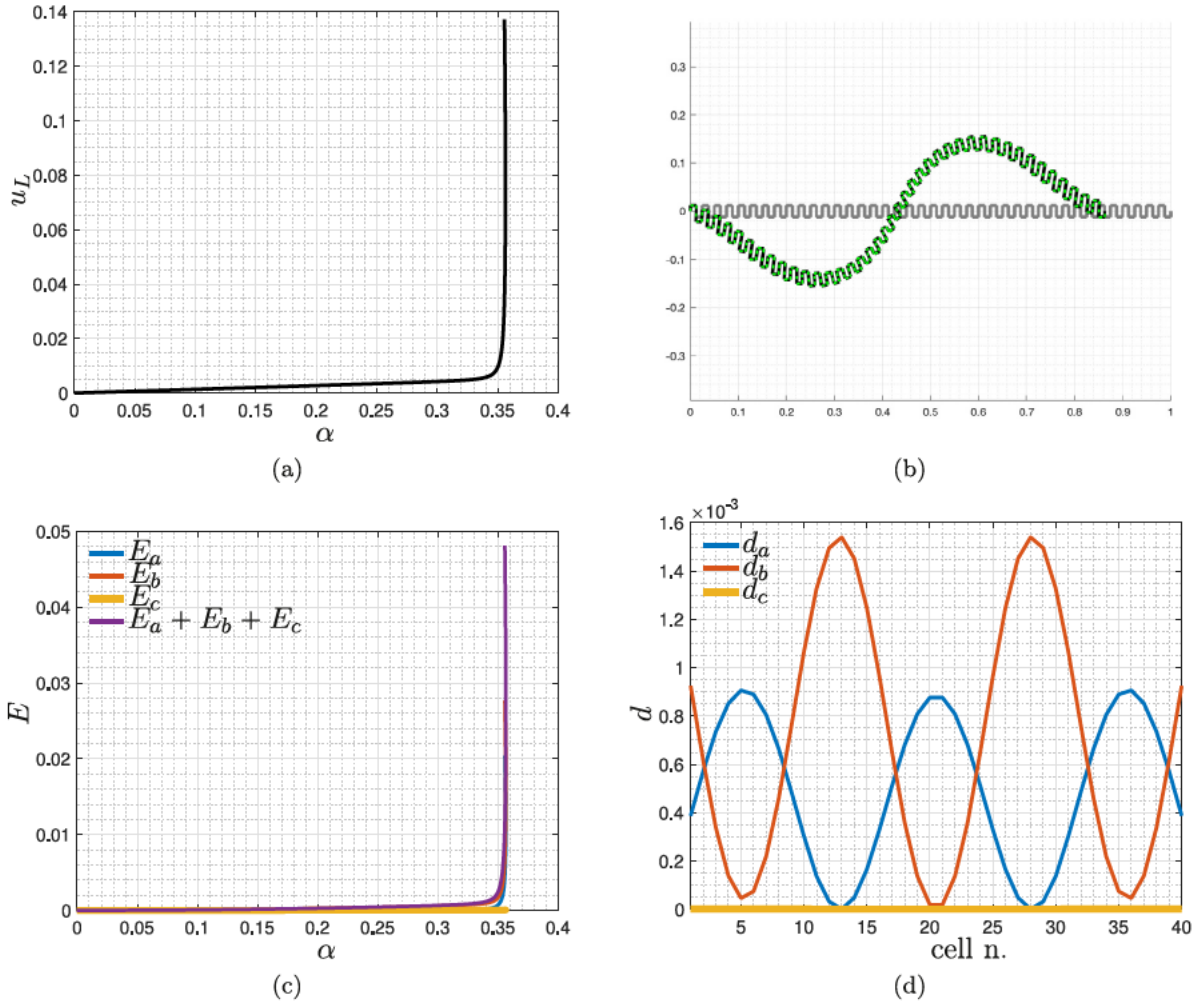

Fig. 22. Duoskelion beam formed by 40 cells subjected to clamp-sliding support kinematic conditions, compression force at the right end-point and modulated transverse perturbation loads at (from the left to the right) 1/4 and 3/4 of the total beam length directed, respectively, downward and upward: equilibrium path (a), final deformation (b), energy evolution (c) and cell energy density (d).

4.5. Cantilever duoskelion beam subjected to mixed traction shearing

In this subsection, cantilever kinematic conditions are considered for the duoskelion beam. Namely, the left extremal midpoint of the duoskelion beam is hinged so to remain fixed. Additionally, the rotation of the corresponding link is enforced to be zero. Thus, any rigid motion of the whole system is avoided. The right extremal midpoint of the duoskelion beam is subjected to a mixed traction shearing loading, with traction and shearing having the same magnitude α.

Fig. 23(a) reports on the equilibrium path of the simply supported duoskelion beam subjected to traction force, being $N_c = 20$. Fig. 23(b) shows the shape of the duoskelion beam with $N_c = 20$ for the last converged step. Fig. 23(c) accounts for deformation energies stored within the duoskelion beam ($N_c = 20$) along the sequence of converged equilibrium steps. Finally, for the last converged solution and $N_c = 20$, Fig. 23(d) shows contributions to the deformation energy for each periodically repeated cell. Figs. 24(a, b, c, d) and 25(a, b, c, d) are analogous to Fig. 23(a, b, c, d), but are referred to $N_c = 40$ and $N_c = 80$, respectively. Figs. 23(b), 24(b), and 25(b) show that midpoints of the duoskelion beam form a line which is bent in a transition zone. Such a transition zone is adjacent to the right extremal midpoint of the duoskelion beam, where ≪ clamping ≫ kinematic conditions are assigned. Rightmost such a transition zone, the duoskelion beam has a straight configuration, directed toward the external applied loading. When N_c increases, it seems that the line formed by mid points be comes increasingly smooth within the transition zone and that the size of such a zone tends to a finite value.

Figs. 23(c), 24(c), and 25(c) show that as N_c increases bending energy becomes increasingly relevant. This observation is corroborated by Figs. 23(d), 24(d), and 25(d). Additionally, these figures suggest that bending energy density per unit line shows an increasingly quick decay with the abscissa, leading to deformation energy being stored mainly within the left transition zone with almost no deformation energy being stored in proximity of the right boundary of the duoskelion beam.

5. Concluding remarks and future challenges

In this work, a recently developed discrete Timoshenko like ele ment has been briefly introduced, as well as the geometry of the duoskelion beam system. Hypotheses have been made for ratios be tween homologous and non homologous stiffnesses within the same cell, that is then periodically repeated. Successively, the numerical scheme employed to solve the static equilibrium problem has been described. Finally, results of numerical tests have been presented. It is concluded that the introduced duoskelion beam is to all intents and purposes a *metamaterial*. Indeed, while it is arguable the definition of metamaterial [48], as a matter of fact the introduced duoskelion beam shows interesting properties that could be exploited in real world applications. Such properties are the overall result of many simple

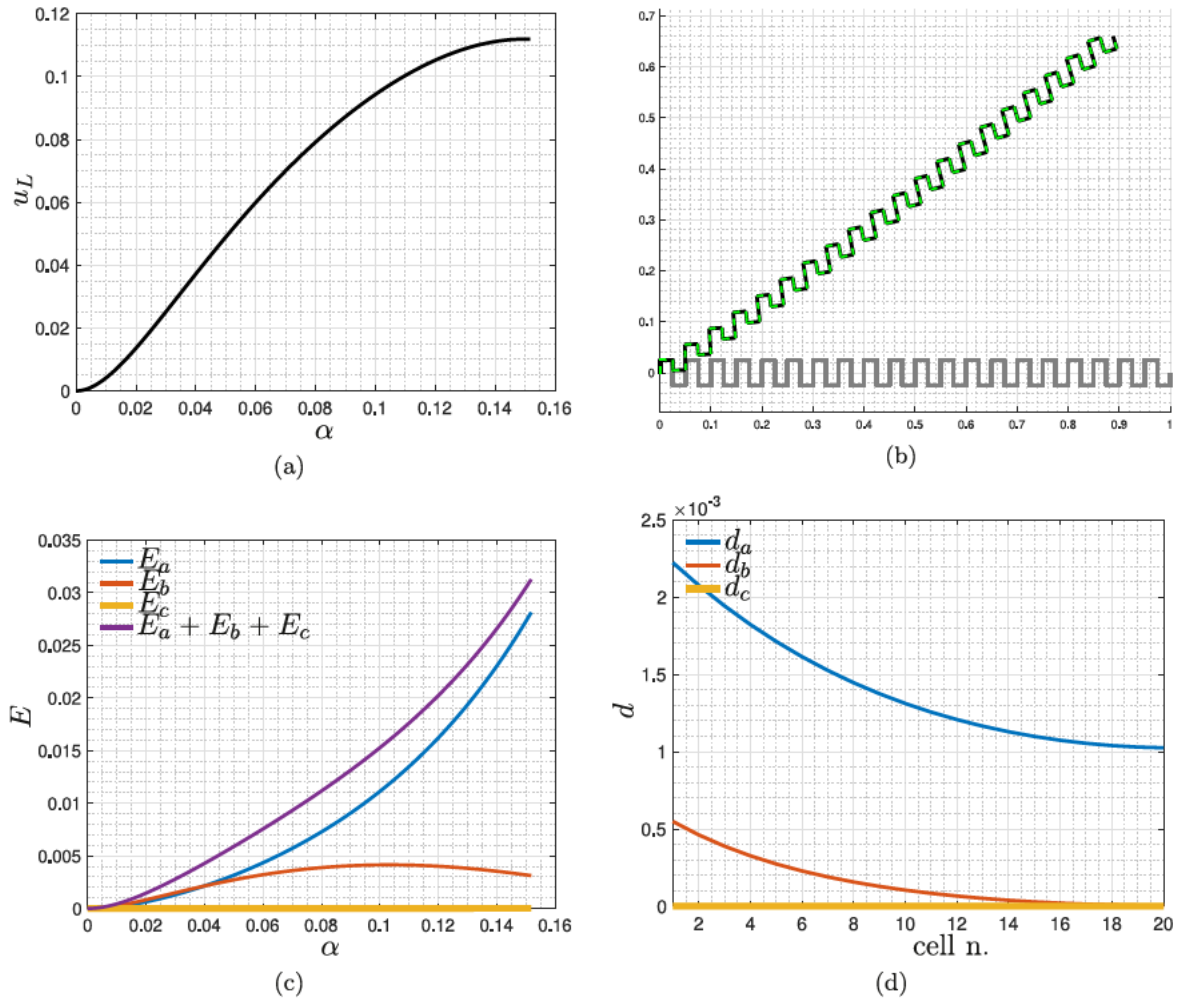

Fig. 23. Cantilever duoskelion beam formed by 20 cells subjected to mixed traction-shearing loading conditions: equilibrium path (a), final deformation (b), energy evolution (c) and cell energy density (d).

interactions occurring at micro scale. Thus as in strain gradient lattices [49,50], swarm robots [51,51], king post like trusses [36,52] and granular assemblies [53 55] in duoskelion beams complex behaviors are observed at macro scale as a result of an ingenious and simple geometrical arrangement at micro scale.

As an instance, duoskelion beams can be used as mechanical switches with customizable *on/off* traction loading threshold, in compression they are capable to strongly couple transverse and axial motions, and they could be designed to show a mono directional response, *i.e.* to be extensible but incompressible, see [56]. Owing to the richness and peculiarity of the mechanical behaviors exhibited by duoskelion beams, it is believed that the mechanics of duoskelion beams deserves to be further analyzed through the many available modeling [57,58] and numerical [57,59,60] strategies. It would be particularly interesting to assess the influence of different asymptotic scalings and to relax the hypotheses on ratios between homologous and non homologous stiffnesses. This last outlook is the main motivation which actually led to using such a (more than needed) sophisticated and refined model: to easily obtain in the future desired structures as special cases, [61] rather than having to re do everything from scratch.

It is worth to remark that an additional objective has been reached through this work, which is to provide evidence that could be useful in guiding and validating asymptotic homogenization of duoskelion beams. Following procedures usually employed in new metamaterials studies, special attention has been given, in exploring the mechanical properties of duoskelion beams, to understanding the local mechanisms that determine their overall behaviors, see [62]. More specifically, emphasis has been given to the study of how and whether or not these mechanisms change when the number of periodically repeated cells blows up to infinite for a fixed total length.

Indeed, such a study is purposely preliminary to future attempts in scale bridging, meaning passing from a discrete micro/meso representation to a macroscopic one valid when then system is made up by many periodically repeated cells. Scale bridging is currently one of the most important challenges in metamaterials mechanics. Indeed, multi scale approaches are nowadays considered to be the most suitable ones to deal with complexity arising from collective simple interactions, [63 65].

In this work, special care has been put in the kinematic description of the system, aimed at avoiding any confusion. Indeed, in plane Timoshenko beam elements thus with a discrete Timoshenko kinematics have been employed to assemble a structure having the duoskelion geometry. Such a structure, via assumptions on ratios between stiffnesses, results into linked rigid bodies, whose kinematics can in turn be given in terms of three parameters each. A convenient and traditional choice for such a kinematic parametrization is given by the displacement of the barycentres (midpoints of the duoskelion beam) of such rigid bodies and their rotation. This suggests that a reasonable macroscopic 1D continuum description of duoskelion beams could be obtained by using Timoshenko kinematics. While this might seem a kind of Russian nesting dolls, such a high care in describing precisely the geometry and kinematics at different scales is very important for

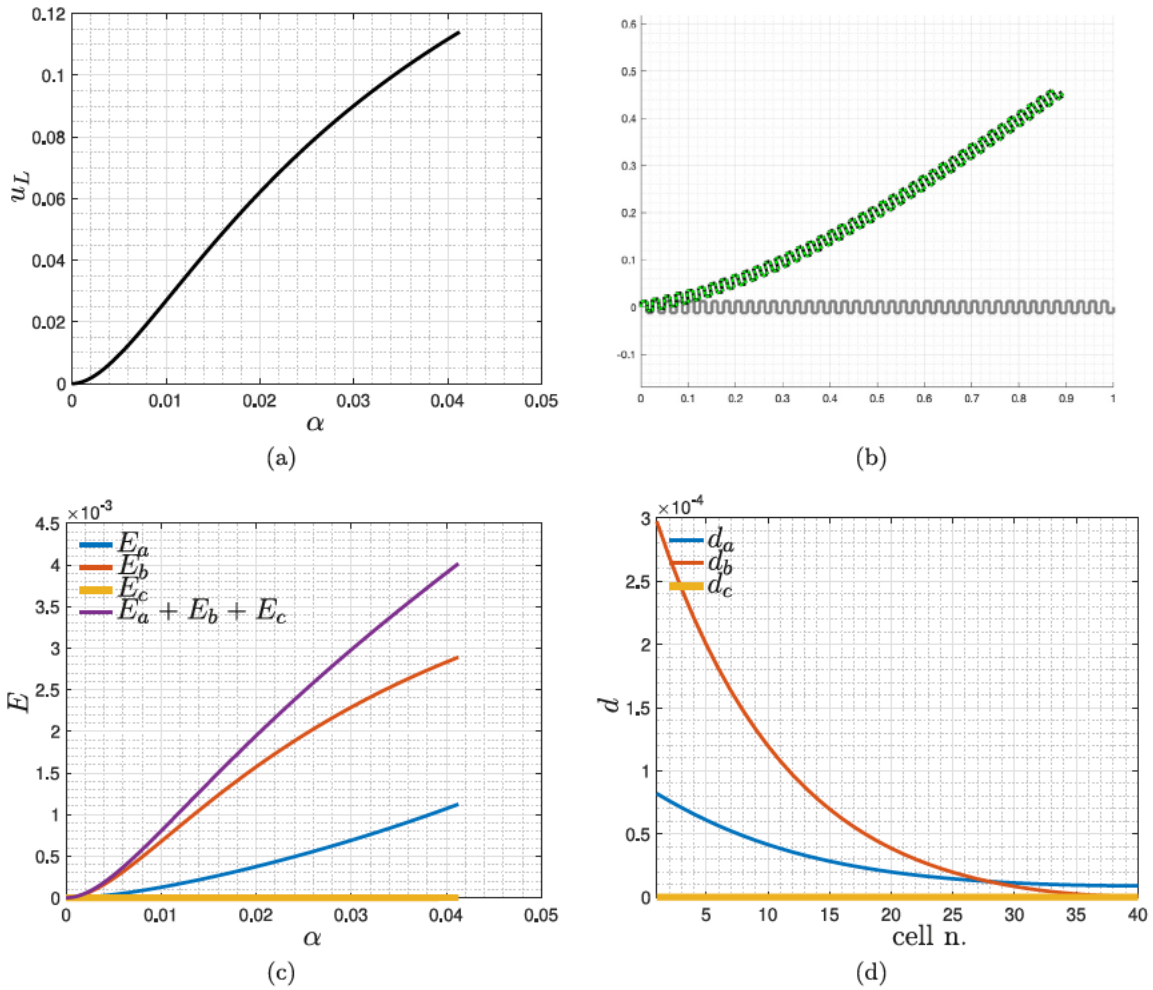

Fig. 24. Cantilever duoskelion beam formed by 40 cells subjected to mixed traction-shearing loading conditions: equilibrium path (a), final deformation (b), energy evolution (c) and cell energy density (d).

discrete to continuum bridging [66], where the identification of stan dard and enriched kinematical fields is necessary to retrieve generalized continuum descriptions [67,68] and to apply consistently multi scale imaging techniques.

Current research work is indeed directed toward interfacing ex perimental measurements obtained by imaging techniques at multiple scales [69] with numerical modeling in a scale consistent and hence kinematically consistent way. As mentioned above, it is envisaged that future attempts in passing from the discrete formulation presented in this work to a 1D macroscopic continuum describing the duoskelion beam as a whole *i.e.* attempts in bridging the gap between discrete and continuum could be performed by using variational asymptotic homogenization techniques, which transfer the discrete description of self similar finite dimensional systems into a continuous formulation by computing the deformation energy limit, for the degrees of freedom of the system tending to infinity.

More particularly, the kinematic descriptors of the continuum are introduced as continuous functions, chosen such that their evaluation at particular points can be related to the generalized coordinates. The deformation energy of the micro model is then formulated using the evaluation of the continuum descriptors at particular points, followed by a Taylor expansion of the energy with respect to the micro length scale, which is proportional to the inverse of the number of periodically repeated cells. Scaling laws for the constitutive parameters in the micromodel are specified followed by a limit process in which the energy of the continuum is retrieved as a limit.

Owing to the recent advances in manufacturing techniques, it is also envisaged that many technologies, materials and design solutions can be fruitfully applied to the realization of duoskelion beams. As an instance, duoskelion beams might be exploited as soft actuated robotic arms in the spirit of [70,71]. In conclusion, it is believed that this work will help and further motivate the mechanics community in shedding light on the behavior of micro structured chiral beams, that are recently attracting the attention of researchers.

Declaration of competing interest

The authors declare that they have no known competing finan cial interests or personal relationships that could have appeared to influence the work reported in this paper.

Acknowledgment

Emilio Barchiesi, Alberto M. Bersani, and Francesco dell'Isola are members of the Gruppo Nazionale per la Fisica Matematica (GNFM) of the Istituto Nazionale di Alta Matematica (INdAM).

Emilio Turco was supported by the University of Sassari, Italy (Fondo di Ateneo per la ricerca 2019). This contribution is gratefully acknowledged.

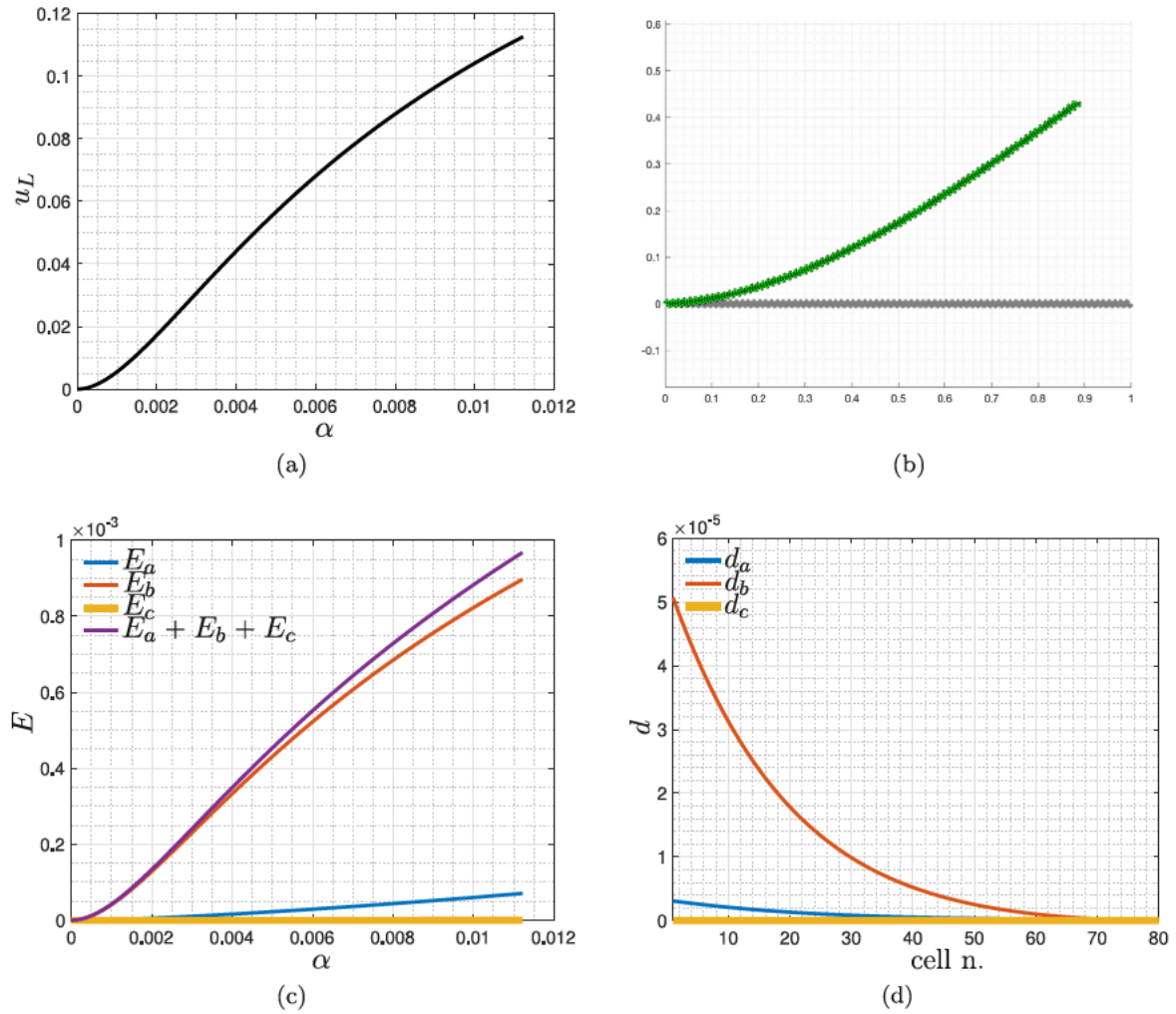

Fig. 25. Cantilever duoskelion beam formed by 80 cells subjected to mixed traction-shearing loading conditions: equilibrium path (a), final deformation (b), energy evolution (c) and cell energy density (d).

References

[1] A. Carcaterra, F. dell'Isola, R. Esposito, M. Pulvirenti, Macroscopic description of microscopically strongly inhomogenous systems: A mathematical basis for the synthesis of higher gradients metamaterials, Arch. Ration. Mech. Anal. 218 (3) (2015) 1239–1262.

[2] S. Eugster, F. dell'Isola, D. Steigmann, Continuum theory for mechanical metamaterials with a cubic lattice substructure, Math. Mech. Complex Syst. 7 (1) (2019) 75–98.

[3] P. Seppecher, J.-J. Alibert, F. dell'Isola, Linear elastic trusses leading to continua with exotic mechanical interactions, J. Phys. Conf. Ser. 319 (1) (2011) 012018.

[4] F. dell'Isola, D. Steigmann, A. Della Corte, Synthesis of fibrous complex structures: Designing microstructure to deliver targeted macroscale response, Appl. Mech. Rev. 67 (6) (2015) 060804.

[5] F. dell'Isola, T. Lekszycki, M. Pawlikowski, R. Grygoruk, L. Greco, Designing a light fabric metamaterial being highly macroscopically tough under directional extension: first experimental evidence, Z. Angew. Math. Phys. 66 (6) (2015) 3473–3498.

[6] F. dell'Isola, P. Seppecher, M. Spagnuolo, E. Barchiesi, F. Hild, T. Lekszycki, I. Giorgio, L. Placidi, U. Andreaus, M. Cuomo, S.R. Eugster, A. Pfaff, K. Hoschke, R. Langkemper, E. Turco, R. Sarikaya, A. Misra, M. De Angelo, F. D'Annibale, A. Bouterf, X. Pinelli, A. Misra, B. Desmorat, M. Pawlikowski, C. Dupuy, D. Scerrato, P. Peyre, M. Laudato, L. Manzari, P. Göransson, C. Hesch, S. Hesch, P. Franciosi, J. Dirrenberger, F. Maurin, Z. Vangelatos, C. Grigoropoulos, V. Melissinaki, M. Farsari, W. Muller, B. Emek Abali, C. Liebold, G. Ganzosch, P. Harrison, R. Drobnicki, L. Igumnov, F. Alzahrani, T. Hayat, Advances in pantographic structures: design, manufacturing, models, experiments and image analyses, Contin. Mech. Thermodyn. 31 (4) (2019) 1231–1282.

[7] F. dell'Isola, P. Seppecher, J.J. Alibert, T. Lekszycki, R. Grygoruk, M. Pawlikowski, D.J. Steigmann, I. Giorgio, U. Andreaus, E. Turco, M. Gołaszewski, N. Rizzi, C. Boutin, V.A. Eremeyev, A. Misra, L. Placidi, E. Barchiesi, L. Greco, M. Cuomo, A. Cazzani, A. Della Corte, A. Battista, D. Scerrato, I. Zurba Eremeeva, Y. Rahali, J.-F. Ganghoffer, W. Muller, G. Ganzosch, M. Spagnuolo, A. Pfaff, K. Barcz, K. Hoschke, J. Neggers, F. Hild, Pantographic metamaterials: an example of mathematically driven design and of its technological challenges, Contin. Mech. Thermodyn. 31 (4) (2019) 851–884.

[8] M. Golaszewski, R. Grygoruk, I. Giorgio, M. Laudato, F. di Cosmo, Metamaterials with relative displacements in their microstructure: technological challenges in 3D printing, experiments and numerical predictions, Contin. Mech. Thermodyn. 31 (4) (2019) 1015–1034.

[9] M. Spagnuolo, P. Peyre, C. Dupuy, Phenomenological aspects of quasi-perfect pivots in metallic pantographic structures, Mech. Res. Commun. 101 (2019) 103415.

[10] F. dell'Isola, T. Lekszycki, M. Spagnuolo, P. Peyre, C. Dupuy, F. Hild, A. Misra, E. Barchiesi, E. Turco, J. Dirrenberger, Experimental methods in pantographic structures, in: F. dell'Isola, D.J. Steigmann (Eds.), Discrete and Continuum Models for Complex Metamaterials, Cambridge University Press, 2020 (Chapter 6).

[11] F. dell'Isola, I. Giorgio, M. Pawlikowski, N.L. Rizzi, Large deformations of planar extensible beams and pantographic lattices: Heuristic homogenisation, experimental and numerical examples of equilibrium, Proc. R. Soc. Lond. A: Math. Phys. Eng. Sci. 472 (2185) (2016) 1–23.

[12] E. Turco, F. dell'Isola, A. Cazzani, N.L. Rizzi, Hencky-type discrete model for pantographic structures: numerical comparison with second gradient continuum models, Z. Angew. Math. Phys. 67 (85) (2016) 1–28.

[13] E. Turco, K. Barcz, M. Pawlikowski, N.L. Rizzi, Non-standard coupled extensional and bending bias tests for planar pantographic lattices. Part I: numerical simulations, Z. Angew. Math. Phys. 67 (122) (2016) 1–16.

[14] E. Turco, K. Barcz, N.L. Rizzi, Non-standard coupled extensional and bending bias tests for planar pantographic lattices. Part II: comparison with experimental evidence, Z. Angew. Math. Phys. 67 (123) (2016) 1–16.

[15] I. Giorgio, P. Harrison, F. dell'Isola, J. Alsayednoor, E. Turco, Wrinkling in engineering fabrics: a comparison between two different comprehensive modelling approaches, Proc. R. Soc. A: Math. Phys. Eng. Sci. 474 (2018) 1–20, (20180063).

[16] M. De Angelo, E. Barchiesi, I. Giorgio, B. Emek Abali, Numerical identification of constitutive parameters in reduced order bi-dimensional models for pantographic structures: application to out-of-plane buckling, Arch. Appl. Mech. 89 (7) (2019) 1333–1358.

[17] E. Turco, Stepwise analysis of pantographic beams subjected to impulsive loads, Math. Mech. Solids (2020) 1–18, http://dx.doi.org/10.1177/1081286520938841.

[18] A. Misra, T. Lekszycki, I. Giorgio, G. Ganzoch, W.H. Müller, F. dell'Isola, Pantographic metamaterials show atypical Poynting effect reversal, Mech. Res. Commun. 89 (2018) 6–10.

[19] M. Laudato, L. Manzari, E. Barchiesi, F. Di Cosmo, P. Göransson, First experimental observation of the dynamical behavior of a pantographic metamaterial, Mech. Res. Commun. 94 (2018) 125–127.

[20] L. Placidi, L. Greco, S. Bucci, E. Turco, N.L. Rizzi, A second gradient formulation for a 2D fabric sheet with inextensible fibres, Z. Angew. Math. Phys. 67 (114) (2016) 1–24.

[21] C. Boutin, F. dell'Isola, I. Giorgio, L. Placidi, Linear pantographic sheets. Asymptotic micro-macro models identification, Math. Mech. Complex Syst. 5 (2) (2017) 127–162.

[22] H. Altenbach, V.A. Eremeyev, On the constitutive equations of viscoelastic micropolar plates and shells of differential type, Math. Mech. Complex Syst. 3 (3) (2015) 273–283.

[23] I. Giorgio, M. De Angelo, E. Turco, A. Misra, A Biot–Cosserat two-dimensional elastic nonlinear model for a micromorphic medium, Contin. Mech. Thermodyn. 32 (2020) 1357–1369.

[24] N. Nejadsadeghi, A. Misra, Extended granular micromechanics approach: a micromorphic theory of degree n, Math. Mech. Solids 25 (2) (2020) 407–429.

[25] F. Hild, A. Misra, F. dell'Isola, Multiscale dic applied to pantographic structures. experimental mechanics, Exp. Mech. (2020) in press.

[26] E. Turco, A. Misra, M. Pawlikowski, F. dell'Isola, F. Hild, Enhanced Piola–Hencky discrete models for pantographic sheets with pivots without deformation energy: numerics and experiments, Int. J. Solids Struct. 147 (2018) 94–109.

[27] I. Giorgio, F. dell'Isola, D.J. Steigmann, Axisymmetric deformations of a 2nd grade elastic cylinder, Mech. Res. Commun. 94 (2018) 45–48.

[28] F. dell'Isola, A. Madeo, P. Seppecher, Cauchy tetrahedron argument applied to higher contact interactions, Arch. Ration. Mech. Anal. 219 (3) (2016) 1305–1341.

[29] L. Placidi, A variational approach for a nonlinear one-dimensional damage-elasto-plastic second-gradient continuum model, Contin. Mech. Thermodyn. 28 (1–2) (2016) 119–137.

[30] V.A. Eremeyev, F.S. Alzahrani, A. Cazzani, F. dell'Isola, T. Hayat, E. Turco, V. Konopińska-Zmysłowska, On existence and uniqueness of weak solutions for linear pantographic beam lattices models, Contin. Mech. Thermodyn. 31 (6) (2019) 1843–1861.

[31] U. Andreaus, F. dell'Isola, I. Giorgio, L. Placidi, T. Lekszycki, N.L. Rizzi, Numerical simulations of classical problems in two-dimensional (non) linear second gradient elasticity, Internat. J. Engrg. Sci. 108 (2016) 34–50.

[32] A. Pisano, A. Sofi, P. Fuschi, Finite element solutions for nonhomogeneous nonlocal elastic problems, Mech. Res. Commun. 36 (7) (2009) 755–761.

[33] L. Greco, An iso-parametric G^1-conforming finite element for the nonlinear analysis of Kirchhoff rod. part I: the 2D case, Contin. Mech. Thermodyn. (2020) http://dx.doi.org/10.1007/s00161-020-(2020)00861-9.

[34] J. Niiranen, V. Balobanov, J. Kiendl, S.B. Hosseini, Variational formulations, model comparisons and numerical methods for Euler–Bernoulli micro- and nano-beam models, Math. Mech. Solids 24 (1) (2019) 312–335.

[35] E. Barchiesi, S.R. Eugster, L. Placidi, F. dell'Isola, Pantographic beam: A complete second gradient 1D-continuum in plane, Z. Angew. Math. Phys. 70 (135) (2019).

[36] J.-J. Alibert, P. Seppecher, F. dell'Isola, Truss modular beams with deformation energy depending on higher displacement gradients, Math. Mech. Solids 8 (1) (2003) 51–73.

[37] I. Giorgio, F. dell'Isola, A. Misra, Chirality in 2d cosserat media related to stretch-micro-rotation coupling with links to granular micromechanics, Int. J. Solids Struct. 202 (2020) 28–38.

[38] A. Misra, N. Nejadsadeghi, M. De Angelo, L. Placidi, Chiral metamaterial predicted by granular micromechanics: verified with 1D example synthesized using additive manufacturing, Contin. Mech. Thermodyn. (2020) 1–17, http://dx.doi.org/10.1007/s00161-020-00862-8.

[39] E. Turco, E. Barchiesi, I. Giorgio, F. dell'Isola, A Lagrangian Hencky-type non-linear model suitable for metamaterials design of shearable and extensible slender deformable bodies alternative to Timoshenko theory, Int. J. Non-Linear Mech. 123 (2020) 103481.

[40] E. Turco, Modelling of two-dimensional Timoshenko beams in Hencky fashion, in: B.E. Abali, I. Giorgio (Eds.), Developments and Novel Approaches in Nonlinear Solid Body Mechanics, in: Advanced Structured Materials, vol. 132, Springer, 2020, pp. 159–177 (Chapter 11).

[41] E. Turco, Discrete is it enough? The revival of Piola–Hencky keynotes to analyze three-dimensional Elastica, Contin. Mech. Thermodyn. 30 (5) (2018) 1039–1057.

[42] N.F. Knight, Finite element techniques for nonlinear postbuckling and collapse of elastic structures, in: Structural Dynamic Systems, Computational Techniques, and Optimization, Gordon and Breach Science Publishers, 1998.

[43] E. Riks, The application of Newton's method to the problem of elastic stability, J. Appl. Mech. Trans. ASME 39 (4) (1972) 1060–1065, Ser E.

[44] M. Fafard, B. Massicotte, Geometrical interpretation of the arc-length method, Comput. Struct. 46 (4) (1993) 603–615.

[45] M.J. Clarke, G.J. Hancock, A study of incremental-iterative strategies for non-linear analyses, Internat. J. Numer. Methods Engrg. 29 (1990) 1365–1391.

[46] P. Wriggers, Nonlinear Finite Element Methods, Springer, 2008.

[47] M. De Angelo, L. Placidi, N. Nejadsadeghi, A. Misra, Non-standard Timoshenko beam model for chiral metamaterial: identification of stiffness parameters, Mech. Res. Commun. 103 (103462) (2020) 1–8.

[48] F. dell'Isola, S. Bucci, A. Battista, Against the fragmentation of knowledge: The power of multidisciplinary research for the design of metamaterials, in: Advanced Methods of Continuum Mechanics for Materials and Structures, in: Advanced Structured Materials, vol. 60, Springer, 2016, pp. 523–545.

[49] H. Abdoul-Anziz, P. Seppecher, Strain gradient and generalized continua obtained by homogenizing frame lattices, Math. Mech. Complex Syst. 6 (3) (2018) 213–250.

[50] H. Abdoul-Anziz, P. Seppecher, Homogenization of periodic graph-based elastic structures, J. Éc. Polytech. Math. 5 (2018) 259–288.

[51] R. dell'Erba, On how swarm robotics can be used to describe particle system's deformation, Contin. Mech. Thermodyn. (2019) 1–21, http://dx.doi.org/10.1007/s00161-019-00845-4.

[52] E. Turco, I. Giorgio, A. Misra, F. dell'Isola, King post truss as a motif for internal structure of (meta)material with controlled properties, R. Soc. Open Sci. 4 (2017) (171153).

[53] E. Turco, In-plane shear loading of granular membranes modeled as a Lagrangian assembly of rotating elastic particles, Mech. Res. Commun. 92 (2018) 61–66.

[54] E. Turco, F. dell'Isola, A. Misra, A nonlinear Lagrangian particle model for grains assemblies including grain relative rotations, Int. J. Numer. Anal. Methods Geomech. 43 (5) (2019) 1051–1079.

[55] A. Misra, T. Matsushima, L. Placidi, Granular material models across scales, Mech. Res. Commun. 102 (2019) 103405.

[56] M. Spagnuolo, Circuit analogies in the search for new metamaterials: Phenomenology of a mechanical diode, in: Nonlinear Wave Dynamics of Materials and Structures, Springer, Cham, 2020, pp. 411–420.

[57] L. Greco, M. Cuomo, L. Contrafatto, A reconstructed local *B* formulation for isogeometric Kirchhoff–Love shells, Comput. Method Appl. Mech. Eng. 332 (2018) 462–487.

[58] V.A. Eremeyev, Strongly anisotropic surface elasticity and antiplane surface waves, Philos. Trans. R. Soc. Lond. A: Math. Phys. Eng. Sci. 378 (2162) (2020) 20190100.

[59] A. Cazzani, M. Malagù, E. Turco, Isogeometric analysis of plane curved beams, Math. Mech. Solids 21 (5) (2016) 562–577.

[60] J. Schulte, M. Dittman, S.R. Eugster, S. Hesch, T. Reinicke, F. dell'Isola, C. Hesch, Isogeometric analysis of fiber reinforced composites using Kirchhoff–Love shell elements, Comput. Method Appl. Mech. Eng. 362 (2020) 112845.

[61] D. Scerrato, I.A. Zhurba Eremeeva, T. Lekszycki, N.L. Rizzi, On the effect of shear stiffness on the plane deformation of linear second gradient pantographic sheets, J. Appl. Math. Mech. / Z. Angew. Math. Mech. 96 (11) (2016) 1268–1279.

[62] E. Turco, A. Misra, R. Sarikaya, T. Lekszycki, Quantitative analysis of deformation mechanisms in pantographic substructures: experiments and modeling, Contin. Mech. Thermodyn. 31 (1) (2019) 209–223.

[63] I. Giorgio, D. Scerrato, Multi-scale concrete model with rate-dependent internal friction, J. Environ. Civil Eng. 21 (7–8) (2017) 821–839.

[64] I. Giorgio, U. Andreaus, F. dell'Isola, T. Lekszycki, Viscous second gradient porous materials for bones reconstructed with bio-resorbable grafts, Extreme Mech. Lett. 13 141–147.

[65] I. Giorgio, U. Andreaus, T. Lekszycki, A. Della Corte, The influence of different geometries of matrix/scaffold on the remodeling process of a bone and bioresorbable material mixture with voids, Math. Mech. Solids 22 (5) (2017) 969–987.

[66] I. Giorgio, N.L. Rizzi, U. Andreaus, D.J. Steigmann, A two-dimensional continuum model of pantographic sheets moving in a 3d space and accounting for the offset and relative rotations of the fibers, Math. Mech. Complex Syst. 7 (4) (2019) 311–325.

[67] B. Emek Abali, W.H. Müller, V.A. Eremeyev, Strain gradient elasticity with geometric nonlinearities and its computational evaluation, Mech. Adv. Mater. Mod. Process. 1 (4) (2015) 1–11.

[68] B. Emek Abali Abali, W.H. Müller, F. dell'Isola, Theory and computation of higher gradient elasticity theories based on action principles, Arch. Appl. Mech. 87 (9) (2017) 1495–1510.

[69] G. Ganzosch, K. Hoschke, T. Lekszycki, I. Giorgio, E. Turco, W.H. Müller, 3d-measurements of 3D-deformations of pantographic structures, Tech. Mech. 38 (3) (2018) 233–245.

[70] I. Giorgio, A discrete formulation of Kirchhoff rods in large-motion dynamics, Math. Mech. Solids (2020) http://dx.doi.org/10.1177/1081286519900902.

[71] I. Giorgio, D. Del Vescovo, Energy-based trajectory tracking and vibration control for multi-link highly flexible manipulators, Math. Mech. Complex Syst. 7 (2) (2019) 159–174.